Bose–Einstein condensation of atomic gases

Frédéric Chevy and Jean Dalibard
Laboratoire Kastler Brossel,
CNRS, UPMC, Ecole normale supérieure,
24 rue Lhomond, 75005 Paris, France

June 16, 2010

The discovery of the superfluid transition of liquid helium [1, 2] marked the first achievement of Bose–Einstein condensation in the laboratory, more than a decade after Einstein's prediction for an ideal gas [3, 4]. Together with superconductivity, they offered the first examples of macroscopic quantum phenomena and as such constituted a milestone in the history of Physics. The quest for the understanding of liquid helium superfluidity was the source of major advances in quantum many-body physics, such as the development of techniques inspired from quantum field theory and Landau's phenomenological two-fluid model. The latter was in particular very successful for describing the hydrodynamics of this quantum liquid.

However, interactions between atoms in liquid helium are strong and make the comparison between experiments and *ab initio* theories a tremendous task. A striking example is the calculation of the critical temperature for the superfluid transition, which was determined only recently by Quantum Monte Carlo simulations [5]. By contrast, gaseous Bose–Einstein condensates (BECs) discovered in 1995 after the development of laser cooling and trapping techniques, constitute weakly interacting systems much closer to Einstein's original idea. The condensation temperature is usually close to the prediction for the ideal gas and more generally, gaseous BECs offer the opportunity to test quantitatively the theoretical ideas elaborated in the past fifty years.

Bose–Einstein condensation has been achieved in dilute gaseous systems either with bosonic atoms [6, 7, 8], or with molecules made with pairs of fermionic atoms [9, 10, 11]. In these dilute systems, the weakness of interactions allows one to adopt a mean-field description in which the many-body wave function $\Psi(\boldsymbol{r}_1, \ldots, \boldsymbol{r}_N)$ is approximated by a factorized state $\varphi(\boldsymbol{r}_1) \ldots \varphi(\boldsymbol{r}_N)$. The macroscopic matter wave $\varphi(\boldsymbol{r})$, which was introduced phenomenologically for liquid helium, provides for atomic gases an accurate description of the microscopic degrees of freedom [12, 13, 14]. As a consequence, ultra-cold atoms allow for a large variety of spectacular phenomena, such as interference between independent condensates [15] and long range phase coherence in an *atom laser* [16].

In this chapter, we present an overview of the specific experimental tools developed in the field of ultra-cold gases to achieve and probe superfluidity in vapours of bosonic atoms.

We first describe the main cooling techniques: the magneto-optical trap, which brings an atomic vapour from room temperature down to the sub-mK range, and the evaporative cooling scheme, which bridges the gap to the superfluid regime. We then proceed to the study of interaction effects. We show that they play a central role in the understanding of both static and dynamic properties of trapped BECs, despite the dilute character of these gases. As a consequence, gaseous BECs and superfluid helium obey the same laws of hydrodynamics and exhibit similar dynamical properties, although their densities differ by several orders of magnitude. The third section is devoted to the coherence properties of gaseous BECs. We show that, by contrast with liquid helium, specific features of ultra-cold gases make them suitable for a direct probing of the quantum coherence associated with Bose–Einstein condensation. Finally, we discuss the possibility of tailoring trapping potentials and realizing low dimensional systems where one or two directions of motion are frozen.

1 Production of a gaseous atomic condensate

Every quantum gas experiment starts with the cooling of a vapour of atoms from room temperature (or even higher) down to the milliKelvin range. The standard tool for this spectacular freezing of atomic motion is laser cooling, which has been developed during the 80's [17, 18, 19]. In this section, we present its basic principle and we show how the very same spontaneous emission processes responsible for cooling also set intrinsic limits preventing one from reaching quantum degeneracy. We then discuss how evaporative cooling strategies based on the selective elimination of the most energetic atoms of the gas overcame this fundamental barrier and led to the observation of the first Bose–Einstein condensates.

1.1 Laser cooling of atomic vapors

Most laser cooling schemes use the radiative forces exerted on atoms by continuous laser beams, with a frequency that is quasi-resonant with an electronic transition of the species of interest. The conceptually simplest scheme is *Doppler cooling*, whose basic principle is recalled in Fig. 1a in the case of a one-dimensional system. Two counterpropagating light beams of frequency $\omega_{\rm L}$ are shined on atoms with a resonance frequency $\omega_{\rm A} > \omega_{\rm L}$. For an atom at rest, the radiation pressure forces exerted by the two beams are balanced and the overall force is zero. For a moving atom this balance is broken. Consider for example an atom moving to the right as in Fig. 1a; the Doppler effect shifts the apparent frequency of the right beam upwards and that of the left beam downwards. Being closer to resonance, the radiation pressure force from the right beam is stronger than that of the left one. The atom thus feels a force opposite to its velocity that damps its motion and that provides the cooling of its translational degree of freedom. Using three pairs of laser beams propagating in independent directions, one can extend this scheme to all three spatial directions, thus creating an *optical molasses* for the atoms. The volume of the optical molasses delimited by the intersection of the laser beams is typically a few centimeter-cubes.
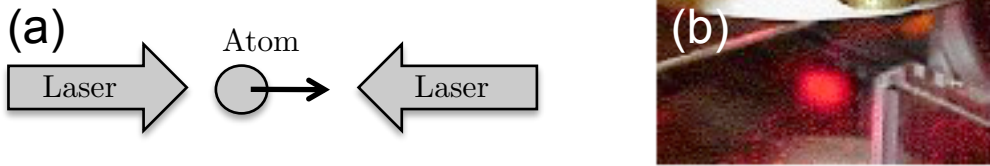
Figure 1: (a) Principle of Doppler cooling in a one-dimensional configuration. The sum of the radiation pressures of two counterpropagating laser beams creates a damping force on a moving atom. (b) Photography of a Lithium magneto-optical trap (photo from Laboratoire Kastler Brossel, ENS Paris). The glowing ball corresponds to $\sim 10^{10}$ atoms trapped at 1 mK.

The equilibrium energy of atoms in an optical molasses results from the balance between the cooling effect that we just described and the heating associated with the random character of spontaneous emission processes. The Brownian motion of the atoms in the molasses can be characterized by a temperature T whose minimal value is $\hbar\Gamma/2k_B$ for Doppler cooling; here Γ is the natural width of the electronic transition excited by the cooling lasers. This temperature is in the range of several hundred microkelvins for alkali atoms, which are the most frequently used species in these experiments. More subtle cooling processes, like *Sisyphus cooling*, also take place in optical molasses and they can lower the temperature down to a few E_R/k_B. Here E_R is the *recoil energy* of an atom when it emits or absorbs a single photon: $E_R = \hbar^2 k_L^2/2m$, where k_L is the wave vector of the laser beams and m the atomic mass. The temperature obtained with Sisyphus cooling is usually in the range 10–100 microkelvins. Note that there also exist subrecoil cooling mechanisms [18], but they are generally not used in quantum gases experiments because of their relatively complex implementation.

1.2 The magneto-optical trap

An optical molasses only provides a damping force on the atoms, but it does not trap them. Because of their Brownian motion in the light beams, the atoms eventually leave the region of the optical molasses in a fraction of a second. This severely limits the number of atoms in the cold gas and its spatial density. To solve this issue, one superimposes to the laser beams a static quadrupolar magnetic field, with the zero of the field in the center of the molasses, thus creating a *magneto-optical trap* (MOT). Due to the spatially varying Zeeman shift of the atomic levels, the radiation pressure force now depends on position. For a proper choice of the polarization of the molasses beams with respect to the local direction of the magnetic field, the radiative pressure not only damps the atomic motion, but also creates a restoring force towards the zero of the magnetic field [20]. The number of atoms at equilibrium in a MOT is in the range 10^8–10^{10}; it depends essentially of the available laser power at the desired wavelength.

For an ideal gas of density n and temperature T, Einstein's criterion for condensation is $n\lambda^3 = \zeta(3/2) \approx 2.6$, where $\lambda = (2\pi\hbar^2/mk_BT)^{1/2}$ is the thermal wavelength and ζ is the Rieman's function [21]. This requires "large" densities and/or low temperatures. A typical target for the density of an ultracold atomic vapour is 10^{14} cm^{-3}. Above this value, the

rate of three-body recombination processes leading to the formation of molecules exceeds 1 s^{-1} and the sample decays before having reached thermal equilibrium. This density is lower than that of liquid helium by 8 orders of magnitude, which brings the degeneracy temperature from the Kelvin region for liquid helium down to 0.1–1 microkelvin for atomic gases. Although the magneto-optical trap is a very powerful tool to bring an atomic vapour in the sub-milliKelvin range, it is not suited for reaching directly quantum degeneracy. The spatial density in a MOT is indeed limited to values much smaller than the target density of 10^{14} cm^{-3} mentioned above, because of the permanent scattering of photons by the trapped atoms. More precisely a fluorescence photon emitted by a given atom can be reabsorbed by another nearby atom, leading to an effective repulsive force between these two atoms. This laser-induced repulsion limits the spatial density in a MOT to values in the range 10^{10}–10^{12} cm^{-3}, corresponding to a phase space density 10^{-4}– 10^{-6} for alkali[1] vapours [24].

1.3   Pure magnetic and pure optical confinements

To circumvent the limit on spatial density imposed in a MOT by light-induced repulsion, and also for lowering further the temperature of the gas, it is necessary to use a non-dissipative confinement. Up to know two kinds of traps, magnetic and optical, have been used successfully in the quest for Bose–Einstein condensation. These two families of traps correspond to relatively shallow potential depths, which are insufficient to trap atoms at room temperature. Therefore a first stage of laser cooling is necessary in all quantum gas experiments, in order to capture room temperature atoms and to reduce their energy down to a level where they can be transferred efficiently to a non dissipative potential.

Magnetic traps.   The first class of non dissipative traps is based on a spatially varying magnetic field $\boldsymbol{B}(\boldsymbol{r})$, and can be used for any atom possessing a non-zero magnetic moment $\boldsymbol{\mu}$. In presence of the magnetic field, the atomic potential energy is $V(\boldsymbol{r}) = -\boldsymbol{\mu} \cdot \boldsymbol{B}(\boldsymbol{r})$. If the motion of the atom is slow enough, the projection $\mu_{\parallel}$ of the magnetic moment along the direction of the magnetic field remains constant. The trapping potential is thus simply $V(\boldsymbol{r}) = -\mu_{\parallel} B(\boldsymbol{r})$. Depending on the sign of $\mu_{\parallel}$, the atom is attracted towards the minima of B ($\mu_{\parallel} < 0$) or towards its maxima ($\mu_{\parallel} > 0$). Due to the structure of Maxwell's equations, only local minima of the modulus of a static magnetic field can exist in a region with no current, which means that only low field seeking spin states corresponding to $\mu_{\parallel} < 0$ can be trapped by a static magnetic field.

Laser dipole traps.   The second class of non dissipative traps uses a laser beam whose frequency ω_{L} is chosen far from the atomic resonance line [25]. Dissipation processes associated with spontaneous emission are then negligible and only virtual scattering of photons is permitted. The electric-dipole interaction of the atom with the laser electric field $E(\boldsymbol{r})$ gives rise to the potential energy $V(\boldsymbol{r}) = -\alpha(\omega_{\text{L}})E^2(\boldsymbol{r})/2$, where α is the dynamical polarisability of the atom. Just like a classical driven oscillator, the sign

---

[1]Larger phase space densities -though not yet at quantum degeneracy- have been achieved in Ytterbium and Strontium MOTs, thanks to the much narrower linewidth of the cooling transition [22, 23].

of α depends on the detuning of the laser with respect to the atomic resonance. For red-detuned light ($\omega_{\mathrm{L}} < \omega_{\mathrm{A}}$), α is positive, while it is negative for blue-detuned light ($\omega_{\mathrm{L}} > \omega_{\mathrm{A}}$), a result that can be recovered easily in Thomson's classical model of the atom. For red-detuned light, the potential energy is minimum at the point(s) where the laser intensity is the highest: a focused laser beam acts as a potential well that keeps the atoms trapped around the focal point. Dipole traps have a large variety of applications, since one can produce laser beams with intensity profiles, hence potential landscapes, of nearly arbitrary shapes. They can for instance be used to engineer periodic potentials, the so-called *optical lattices* (see the Chapter by Tin-Lu Ho in this book), or strongly confine atoms in one or two dimensions to a point where the atomic motion is frozen in these directions, thus realizing a quasi two-dimensional or one-dimensional system (see § 4).

1.4 Evaporative cooling to the degenerate regime

Up to now, evaporative cooling is the only path to cool an atomic vapour down to the quantum degenerate regime. Although several implementations exist, the principle of evaporative cooling is always the same: one removes atoms carrying a large energy from the trap, so as to decrease the mean energy - hence the temperature - of the remaining particles. This is achieved by truncating the trapping potential at some energy U_0. A key ingredient in the process is the elastic collision rate that fixes the speed at which atoms are removed from the trap, hence the cooling rate dT/dt [26, 27].

Basic evaporative cooling suffers from the fact that as the temperature decreases, fewer particles reach an energy larger than U_0 and the evaporation process slows down. To circumvent this problem, one turns to *forced evaporative cooling*, obtained by continuously decreasing U_0 in order to keep the ratio $\eta = U_0/k_{\mathrm{B}}T$ constant. When the initial collision rate is large enough, one reaches a runaway regime in which the collision rate increases as the gas gets colder and denser. The quantum degenerate regime is reached after an evaporation time corresponding to a few hundred elastic collisions per atom. During the evaporation process the number of atoms is divided by a factor 100 to 1000. The number of atoms at the condensation point ranges between 10^3 and 10^8, depending on the initial loading of the magnetic trap, on the optimisation of the evaporation process and on the subsequent goal of the experiment.

In a magnetic trap, evaporation is performed using a radio-frequency (rf) electromagnetic field of frequency ν_{rf} that flips the atom spin to a non-trapped state. Since the trapping magnetic field $\boldsymbol{B}$ depends on position, the expulsion only takes place at positions $\boldsymbol{r}$ where the resonance condition $h\nu_{\mathrm{rf}} = g_{\mathrm{L}}\mu_{\|}B(\boldsymbol{r})$ is satisfied, where g_{L} is the Landé factor of the relevant internal atomic state (Figure 2a). By sweeping ν_{rf} one can thus produce the desired change of U_0 without changing the characteristics of the trap itself.

In a laser dipole trap, all spin states feel the same potential and rf evaporation cannot be used. In this case one takes advantage of the relation between the depth of the trapping potential and the intensity of the laser light shined on the atoms: forced evaporation is obtained simply by decreasing the laser power. One drawback of this scheme is that the trapping strength also decreases during the evaporation, which diminishes the collision

rate that is so crucial for the success of evaporation. The criterion on the initial collision rate for a successful evaporation is therefore more stringent in a dipole trap than in a magnetic trap[2].

Evaporative cooling of atoms in a magnetic trap led in 1995 to the first observation of a Bose–Einstein condensate of Rubidium atoms by the group of E. A. Cornell and C. Wieman in Boulder [6, 28], soon followed by the groups of W. Ketterle at MIT with Sodium atoms [7, 29], and of R. Hulet in Houston with Lithium atoms [8]. Evaporation down to the degenerate regime in a pure optical trap was achieved in 2001 by the group of M. S. Chapman [30]. In Fig. 2b we show images of the momentum distribution of the first Bose–Einstein condensates obtained at JILA in 1995. The momentum distribution was obtained by taking a picture after releasing the atoms from their trap. For low atom numbers, interactions are negligible and the gas expands freely[3]. In this case, the density profile after time of flight is proportional to the initial momentum distribution. The onset of Bose–Einstein condensation is clearly observed by the appearance of a narrow peak in the momentum distribution, corresponding to the macroscopic accumulation of atoms in the single particle ground state of the trap.

In practice, the atoms are observed by absorption imaging, a process in which one shines a resonant beam on the cloud and images the cast shadow on a CCD camera. The drawback of this method is that it destroys the cloud and forbids real time imaging of its dynamics. An alternative method uses a non resonant probe beam, which is practically not absorbed by the cloud of atoms but simply dephased. By using a phase contrast technique, also used in standard microscopy to image transparent objects, it is possible to reconstruct the refractive index profile of the cloud, hence its density profile.

1.5   Bose–Einstein condensation in a trap

In order to calculate the critical temperature for a Bose gas confined by a potential $V(\boldsymbol{r})$, one often starts with the semi-classical approximation, which states that the phase space density of an ideal gas of chemical potential μ and temperature T reads:

$$f(\boldsymbol{p}, \boldsymbol{r}) \approx \frac{1}{(2\pi\hbar)^3} \frac{1}{e^{\beta(h(\boldsymbol{p},\boldsymbol{r})-\mu)} - 1} \ . \tag{1}$$

Here $\beta = 1/k_\mathrm{B}T$ and $h(\boldsymbol{p}, \boldsymbol{r}) = p^2/2m + V(\boldsymbol{r})$ is the classical Hamiltonian for a particle of mass m trapped in the potential V. The semi-classical approximation is valid as soon as the size of the cloud is larger than other characteristic length scales, such as the spatial extent of the ground state wave function in the trap or the thermal wavelength λ.

For simplicity we restrict from now on to the case of a harmonic potential with frequencies ω_i, $i = x, y, z$ and $V(0) = 0$. As in free space, the chemical potential can take

---

[2]Note that it is also possible to recover a fully efficient evaporation in a dipole trap by refocusing the laser beam on the atoms as the evaporation proceeds, so as to maintain a constant trapping strength like in a magnetic trap.

[3]Although this situation was indeed achieved for the first gaseous BECs, we will see below that in most cases, interactions actually play a crucial role in the equilibrium shape and in the dynamics of the condensate.
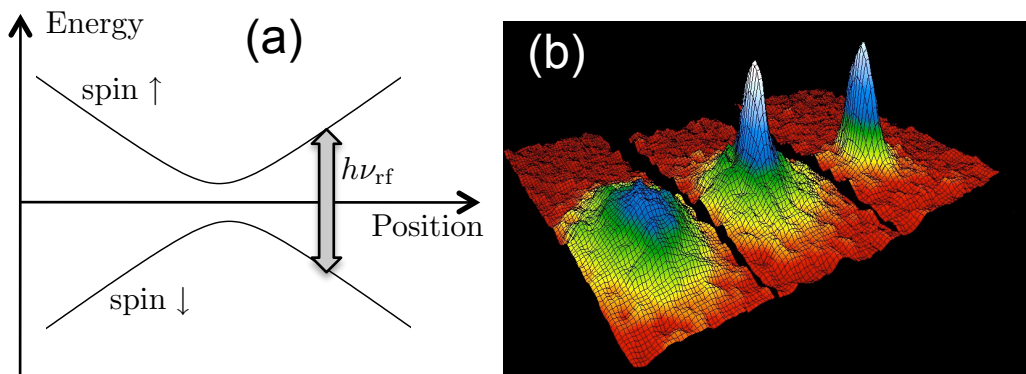
Figure 2: (a) Evaporative cooling in a magnetic trap, using a radio-frequency that flips the magnetic moment of atoms at a given position in the trap. (b) First observation of a gaseous Bose–Einstein condensate (photos: courtesy of Eric Cornell, NIST Boulder). For the left to the right, the three density profiles correspond to decreasing temperatures. The first one is still in the classical regime, where the density distribution is given by the classical Boltzmann law. The last one corresponds to a quasi-pure condensate.

only non positive values, and the phase space density is at any place smaller than its value for $\mu = 0$. For a given temperature, the number of atoms that can be accounted for with the semi-classical result (1) is bounded from above by

$$N_{\text{max}} = \int \frac{1}{e^{\beta h(\boldsymbol{p},\boldsymbol{r})} - 1} \frac{d^3r\, d^3p}{(2\pi\hbar)^3} = \zeta(3) \left(\frac{k_B T}{\hbar\bar{\omega}} \right)^3 , \qquad (2)$$

where $\zeta(3) \approx 1.2$ and $\bar{\omega}^3 = \omega_x \omega_y \omega_z$. When the atom number is larger than N_{max}, atoms in excess accumulate in the ground state of the trap, following the general Bose–Einstein condensation scenario. Conversely for a given atom number N, the condensation occurs when the temperature passes below the critical value T_c such that $k_B T_c = \hbar\bar{\omega}(N/\zeta(3))^{1/3}$.

Within the semi-classical approximation, the threshold for condensation in a trap is directly related to the critical point of a homogeneous system. To prove this point we first note that the density at the center of the trap $n(0)$ can be calculated from the expression (1) for the phase space density. Suppose now that the number of atoms in the trap is equal to the maximal value given in (2). One readily finds that $n(0) = n_c$ where $n_c = \zeta(3/2)\lambda^{-3}$ is the critical density for Bose–Einstein condensation in a homogenous system.

So far we considered only the case of an ideal gas. To go further, one needs a proper modelling of the interaction potential $U(\boldsymbol{r})$ between a pair of atoms separated by a distance $\boldsymbol{r}$. This modelling can be written in a simple form, thanks to the fact that at low temperature, the thermal wavelength is larger than the range of the interatomic potential. One can therefore replace the (complicated) true potential by a contact interaction, with a strength g proportional to the two-body scattering length a_s:

$$U(\boldsymbol{r}) = g\,\delta(\boldsymbol{r}) \qquad \text{with} \qquad g = \frac{4\pi\hbar^2 a_s}{m} . \qquad (3)$$

In the rest of this paper we will use this simple modelling of atomic interactions, except in § 2.5, where we will address the case of long range (dipolar) forces.

Trapped atomic gases being very dilute at least for $T > T_c$, the influence of interactions on the critical point is relatively weak. The main effect is that because of repulsive (respectively attractive) interactions, the density at the center of the trap for a given number of atoms is lower (resp. higher) than its value in absence of interactions. Therefore one needs to place more (resp. less) atoms in the trap in order to reach the threshold $n(0)\,\lambda^3 = \zeta(3/2)$. This can be expressed as a shift of the critical temperature [31]

$$\frac{\delta T_c}{T_c} \approx -1.33\, N^{1/6}\, \frac{a_s}{a_{ho}},\tag{4}$$

where $a_{ho} = \sqrt{\hbar/m\bar{\omega}}$ is the extension of the ground state wave function in a harmonic potential of frequency $\bar{\omega}$. For typical situations, the scattering length a_s is at the nanometer scale, whereas a_{ho} is at the micrometer scale. Therefore the relative shift of T_c is usually a few percents. Its measurement is described in [32], where corrections to T_c due to atom correlations are also reviewed and discussed.

2   Probing a condensate: the hydrodynamic approach

Typical densities in quantum degenerate vapors are typically in the range 10^{13}–10^{14} atoms/cm^3, five to six orders of magnitudes more dilute than air. However, despite this extreme dilution, the dynamics of Bose–Einstein condensates follow the classical laws of hydrodynamics for inviscid fluids. We investigate the low energy modes arising from this hydrodynamic behaviour and show how they were confirmed with a remarkable accuracy by experiments.

2.1   Hartree approximation and Gross–Pitaevskii equation

Compared to liquid helium, ultra-cold gases have a very small density and they can often be considered as systems as independent particles, with quasi-negligible correlations between the atoms. In this respect, these gases are close to the situation discussed by Einstein in his seminal work [3, 4]. The quasi-independence between the atoms in a cold gas is illustrated by the fact that the condensed fraction – defined as the largest eigenvalue of the one-body density matrix – can be close to 100% at very low temperature, whereas it never exceeds 10% in superfluid liquid helium.

To exploit this absence of correlation between the atoms of the gas, a simple and useful approach is the *Hartree approximation*, which consists in describing the many-body wavefunction of a condensate containing N particles by the product

$$\Psi(\boldsymbol{r}_1, \boldsymbol{r}_2, ...\boldsymbol{r}_N, t) = \prod_{i=1}^{N} \varphi(\boldsymbol{r}_i, t),\tag{5}$$

where φ is the macroscopic wave-function describing the behavior of the system. For particles of mass m interacting through a two-body potential $U(\boldsymbol{r}_1, \boldsymbol{r}_2)$ and trapped in an external potential $V(\boldsymbol{r}_1)$, the evolution of φ can be obtained by the minimization of the

action associated with the Lagrangian density

$$\mathcal{L} = -i\hbar\Psi^*\partial_t\Psi + \sum_{i=1}^{N}\left(\frac{\hbar^2}{2m}|\boldsymbol{\nabla}_i\Psi|^2 + V(\boldsymbol{r}_i)|\Psi|^2\right) + \frac{1}{2}\sum_{i,j=1}^{N}U(\boldsymbol{r}_i,\boldsymbol{r}_j)|\Psi|^2. \tag{6}$$

Writing the Euler-Lagrange equations with the Hartree anzatz (5) finally yields the Gross–Pitaevskii equation [33, 34]

$$i\hbar\partial_t\varphi = -\frac{\hbar^2}{2m}\nabla^2\varphi + V(\boldsymbol{r})\varphi(\boldsymbol{r},t) + (N-1)\int U(\boldsymbol{r},\boldsymbol{r}')\,|\varphi(\boldsymbol{r}',t)|^2\,\varphi(\boldsymbol{r},t)\,d^3r'\ . \tag{7}$$

This equation has a clear physical interpretation: each particle in the state $\varphi(\boldsymbol{r},t)$ evolves in a potential that is the sum of the external trapping potential $V(\boldsymbol{r})$ and the mean-field interaction energy due to the $N-1$ remaining particles. In the following we will assume $N \gg 1$, hence we will replace $N-1$ by N.

In most experimental situations[4], the range of the interatomic potential U is much shorter that other relevant length scales, like the interatomic distance or the thermal wavelength. Then, as explained in § 1.5, we can replace U by a contact potential $g\,\delta(|\boldsymbol{r}-\boldsymbol{r}'|)$, and the Gross–Pitaevskii equation turns into the non-linear-Schrödinger equation

$$i\hbar\partial_t\varphi = -\frac{\hbar^2}{2m}\nabla^2\varphi + V(\boldsymbol{r})\varphi(\boldsymbol{r},t) + Ng\,|\varphi(\boldsymbol{r},t)|^2\,\varphi(\boldsymbol{r},t). \tag{8}$$

In the case where the gas is kept in a flat ($V = 0$) cubic box of size L, one can look for stationary solutions of the Gross–Pitaevskii equation with the form $\varphi_0(t) = e^{-i\mu t/\hbar}/L^{3/2}$, where μ is the chemical potential of the system[5]. The resolution is straightforward and yields

$$\mu = gn_0, \tag{9}$$

where $n_0 = N/L^3$ is the particle density in the condensate.

2.2   The Bogoliubov spectrum of collective excitations

Due to the non-linear nature of the Gross–Pitaevskii equation, its resolution for arbitrary initial conditions can be obtained only numerically. However, when the system is weakly perturbed, a first order expansion can be performed. In this section we restrict to the case of a gas confined in a cubic box of size L for which the linearization of the Gross–Pitaevskii and the research of its eigenmodes is relatively simple.

We start by writing $\varphi(\boldsymbol{r},t) = e^{-i\mu t/\hbar}[1+\delta\varphi(\boldsymbol{r},t)]/L^{3/2}$, so that we obtain at first order in $\delta\varphi$ the linear system

$$i\hbar\partial_t\begin{pmatrix}\delta\varphi\\\delta\varphi^*\end{pmatrix} = \mathcal{L}_{GP}\begin{pmatrix}\delta\varphi\\\delta\varphi^*\end{pmatrix} \tag{10}$$

---

[4]The most notable exception being dipolar gases discussed in Sec. 2.5.

[5]One can check that the value of μ obtained with this definition coincides with the energy required to add a Nth particle to the gas containing already $N-1$ atoms.

with the linear operator $\mathcal{L}_{GP}$ given by

$$\mathcal{L}_{GP} = \begin{pmatrix} -\hbar^2 \nabla^2/2m + gn_0 & gn_0 \\ -gn_0 & \hbar^2 \nabla^2/2m - gn_0 \end{pmatrix}. \tag{11}$$

Using translational invariance, solutions of Eq. (10) can be expanded on a set of plane waves $(u_k, v_k)e^{i(\boldsymbol{k}\cdot\boldsymbol{r}-\omega t)}$ diagonalizing the operator $\mathcal{L}_{GP}$ (the so-called Bogoliubov modes). A simple algebra then yields

$$\begin{pmatrix} u_k \\ v_k \end{pmatrix} \propto \begin{pmatrix} \cosh\theta_k \\ \sinh\theta_k \end{pmatrix}, \qquad \tanh 2\theta_k = \frac{1}{k^2\xi^2 + 1}, \tag{12}$$

with the Bogoliubov dispersion relation

$$\omega_k = \sqrt{gn_0 k^2/m \ + \ (\hbar k^2/2m)^2} \ . \tag{13}$$

Here we introduced the *healing length* $\xi = (8\pi n_0 a_{\mathrm{s}})^{-1/2}$, which characterises the distance over which the condensate recovers its homogeneous density when one applies a local perturbation. Note that we implicitly assumed that the scattering length a_{s} is positive, corresponding to an effective repulsive interaction between atoms. In this case, ω is real for any value of k.

The Bogoliubov approximation is valid in the dilute limit $n_0 a_{\mathrm{s}}^3 \ll 1$, or equivalently $n_0 \xi^3 \gg 1$. The Bogoliubov modes describe the low-energy excitations of a Bose-condensed gas, and they can be used to study its low-temperature thermodynamic properties. For instance, the quantum fluctuations of the Bogoliubov modes give access to the quantum depletion of the condensate, i.e. the difference at zero temperature between the total density n and the condensed density n_0. They also provide the first beyond mean-field corrections of the zero temperature equation of state (9) [35].

The dispersion relation (13) displays two different asymptotic regimes. For $k\xi \gg 1$, one recovers the single particle dispersion $\omega \sim \hbar k^2/2m$, as for a non interacting gas. For $k\xi \ll 1$, the dispersion relation is linear, $\omega \sim k\sqrt{gn_0/m}$, and in this regime we can identify the eigenmodes as acoustic waves with sound velocity $c_{\mathrm{s}} = \sqrt{gn_0/m}$.

In gaseous BECs, the Bogoliubov spectrum can be studied by Raman scattering experiments in which two laser beams (labelled 1 and 2) with different frequencies and wave-vectors are shined on the atoms. Let us consider a process where one photon of the beam 1 is transferred to the beam 2 in an "absorption- stimulated emission" cycle (Figure 3a). From energy-momentum conservation this process is associated with the creation of a Bogoliubov excitation of momentum $\boldsymbol{k} = \boldsymbol{q}_1 - \boldsymbol{q}_2$ and frequency $\omega_{\boldsymbol{k}} = \omega_1 - \omega_2$. This can only happen when the condition $\omega_{\boldsymbol{q}_1 - \boldsymbol{q}_2} = \omega_1 - \omega_2$ is satisfied. Therefore, for a given set of directions $(\boldsymbol{q}_1, \boldsymbol{q}_2)$, the rate of Raman scattering varies resonantly with $\omega_1 - \omega_2$, providing one point on the dispersion curve $\omega(k)$. The experiment is then repeated for other directions $(\boldsymbol{q}_1, \boldsymbol{q}_2)$, to map the complete dispersion curve. Strictly speaking, the formalism developed above do not apply as such to the case of trapped gases, because the presence of the confining potential breaks the translational symmetry that led to the modes given in (12). However, the gas can be considered as quasi-homogeneous on length scales much smaller than the cloud size R, and the Bogoliubov spectrum (13) is therefore relevant if one restricts to short wavelength excitations satisfying $kR \gg 1$.
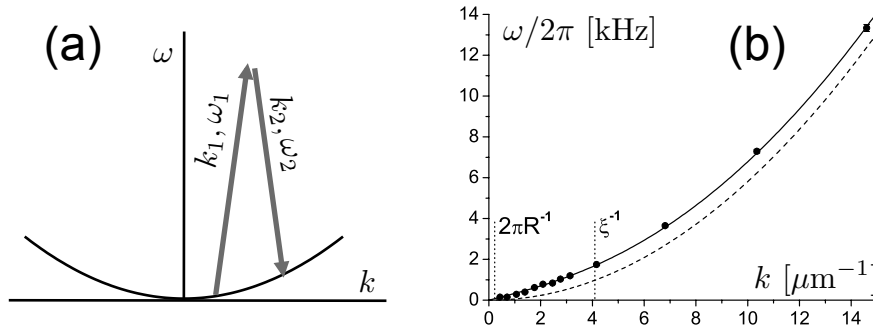
Figure 3: (a) Example of a Raman scattering process, in which a photon of wave vector $\boldsymbol{k}_1$ and frequency ω_1 disappears, and a photon of wave vector $\boldsymbol{k}_2$ and frequency ω_2 is created. (b) Dots: Experimental measurement of the Bogoliubov spectrum in a Rubidium condensate using Raman spectroscopy. The solid and dashed line correspond to the Bogoliubov and free particle spectra, respectively (data from [36]).

We show in Fig. 3b results obtained with this technique by the group of N. Davidson at the Weizmann Institute [36]. The experiment was performed with Rubidium atoms and led to results in excellent agreement with the Bogoliubov dispersion relation (13). Interestingly the excitation spectrum of a gaseous Bose–Einstein is simpler than that of liquid helium, which exhibits a *roton branch* associated with a local minimum of ω_k. This is due to the fact that a cloud of ultra-cold atoms is a weakly interacting system, for which the mean-field approximation adopted here is quite accurate. In recent experiments, the group of E. Cornell at JILA started to explore the strongly interacting regime $na_{\mathrm{s}}^3 \sim 1$ [37] and could observe deviations from the Bogoliubov dispersion relation (13), indicating the breakdown of the mean-field approximation.

The case of attractive interactions. The scattering length a_{s} describing atomic interaction at low energy is negative for some atomic species, like ⁷Li atoms in their lowest energy state. When this occurs, the Bogoliubov dispersion relation (13) leads to imaginary values for ω_k. This feature is the signature of an instability of the gas that collapses under the effect of attractive interactions. For a gas confined in a harmonic potential this collapse was indeed observed, when the number of atoms exceeded a threshold value [38]. In a one-dimensional geometry, this instability is connected to the existence of solitonic solutions of the stationary Gross–Pitaevskii equation[6], which were also observed experimentally with Bose–Einstein condensates of ⁷Li [40, 41]. These coherent atomic 'packets' propagate without deformation, due to a balance between the interaction-induced collapse, and the broadening of their wave-function due to the dispersive nature of the single particle dispersion relation $\omega = \hbar k^2/2m$. This phenomenon is also well known in other domains of physics (in particular hydrodynamics and non-linear optics [42]).

---

[6]Note that solitonic solutions exist also for $g > 0$. In this case, they correspond to a dip in the density profile, and are therefore called dark (or grey when the contrast is not 100%) solitons [39].

2.3 Equilibrium shape and eigenmodes of a trapped condensate

In the presence of a harmonic trapping potential $V(\boldsymbol{r})$, the resolution of the Gross–Pitaevskii equation is more involved than for a homogeneous system. We consider first the equilibrium state of the condensate, setting $\varphi(r,t) = \varphi_0(r)\, e^{-i\mu t/\hbar}$ in (8). In the absence of interactions ($g = 0$), the lowest energy solution $\varphi_0(r)$ is the single-particle ground state in the harmonic trap, i.e. a Gaussian function with an extension $a_{\mathrm{ho}} = (\hbar/m\omega)^{1/2}$ and a chemical potential $\mu = 3\hbar\omega/2$ (for simplicity we assume here an isotropic confinement of frequency ω). In the case where the scattering length is positive, repulsive interactions increase the size R of the cloud. In the limit of large atom numbers, the kinetic energy $\sim \hbar^2/mR^2$ can be neglected with respect to the trapping energy $\sim m\omega^2 R^2$. In this so-called *Thomas–Fermi* regime, the stationary Gross–Pitaevskii equation leads to [43]

$$\mu = g n_0(\boldsymbol{r}) + V(\boldsymbol{r}) \ , \tag{14}$$

where $n_0(\boldsymbol{r}) = N|\varphi_0(\boldsymbol{r})|^2$ is the atom density. This relation yields readily the density profile of the cloud in the presence of the external potential. It can be recovered from (9) using the *local density approximation*, where one considers that the system is locally homogeneous, with a space dependent chemical potential $\mu_{\mathrm{loc}}(\boldsymbol{r}) = \mu - V(\boldsymbol{r})$. For a condensate with N atoms in a harmonic potential, (14) entails that the density distribution is an inverted parabola. The radius of the distribution is given by $R = a_{\mathrm{ho}}\, \eta^{1/5}$ and the chemical potential is $\mu = \hbar\bar{\omega}\, \eta^{2/5}/2$, where we set $\eta = 15 N a_{\mathrm{s}}/a_{\mathrm{ho}}$; the Thomas–Fermi approximation is valid if $R \gg a_{\mathrm{ho}}$, i.e. $\eta \gg 1$.

A similar approach can be followed in the dynamical regime, in which one recovers equations analogous to Euler's equation in classical hydrodynamics. We start by writing the condensate wave function as $\varphi(\boldsymbol{r},t) = \sqrt{n(\boldsymbol{r},t)/N}\, e^{i\theta(\boldsymbol{r},t)}$ (Madelung transform). Expressing the Gross–Pitaevskii equation in terms of the real variables θ and n, we obtain the set of equations

$$\partial_t n \ = \ -\boldsymbol{\nabla} \cdot (n\boldsymbol{v}) \tag{15}$$

$$m\, \partial_t \boldsymbol{v} \ = \ -\boldsymbol{\nabla}\left(g n + V + \frac{m v^2}{2} - \frac{\hbar^2}{2m\sqrt{n}}\nabla^2\sqrt{n}\right), \tag{16}$$

where $\boldsymbol{v}(\boldsymbol{r},t) = \hbar\boldsymbol{\nabla}\theta/m$ is the velocity field of the condensate. The physical interpretation of these two equations is straightforward. The first one expresses the mass conservation, the second one is the Euler equation for an inviscid fluid with an irrotational flow, with θ playing the role of the velocity potential. The term proportional to $\hbar^2$ arises from quantum fluctuations and is called *quantum pressure*. In the semi-classical limit $\hbar \to 0$, it can be neglected and the above set of equations becomes

$$\partial_t n \ = \ -\boldsymbol{\nabla} \cdot (n\boldsymbol{v}) \tag{17}$$

$$m\, \partial_t \boldsymbol{v} \ = \ -\boldsymbol{\nabla}\left(g n + V + m v^2/2\right), \tag{18}$$

which can identified with the Euler equations for a gas of pressure P characterized by the simple equation of state $P = gn$.

A quick inspection shows that the hydrodynamic regime described by the equations (17-18) is valid in the Thomas-Fermi regime $g\bar{n}/\hbar\omega \gg 1$, where $\bar{n}$ is the typical atomic

density in the trap. Interestingly, this criterion is much less stringent than the condition for reaching the hydrodynamic regime for a *classical* trapped gas: $\gamma = \bar{n}\sigma\bar{v}/\omega \gg 1$. The latter condition compares the trap oscillation frequency ω to the collision rate $\bar{n}\sigma\bar{v}$, where $\sigma = 8\pi a_{\mathrm{s}}^2$ is the s-wave scattering cross-section and $\bar{v}$ is the characteristic atomic velocity. In a Bose–Einstein condensate, the velocity is small and is Fourier-limited with $\bar{v} \sim \hbar/mR$, where R is the cloud size. We then find that

$$\gamma \sim \frac{a_{\mathrm{s}}}{R}\left(\frac{g\bar{n}}{\hbar\omega}\right) \ . \tag{19}$$

In typical experimental conditions, $g\bar{n}/\hbar\omega \sim 10$ and the Thomas-Fermi condition is fulfilled. On the contrary, although scattering lengths can be rather large compared to typical atomic lengths (for rubidium it is ~ 5 nm, i.e. 100 times bigger than the Bohr radius), their values are still much lower than the cloud radius $R \sim 10$ μm and the validity condition $\gamma \gg 1$ for reaching the classical hydrodynamic regime is not fullfilled . We thus see that, contrary to classical fluids, hydrodynamicity in quantum gases is not driven by collisions, but by quantum coherence entailing the existence of a one-body wave-function that encapsulates the macroscopic properties of the system.

The resolution of this set of equations in the case of low lying excitation modes in an harmonic trap has been the subject of a large amount of both theoretical and experimental work [13, 14]. For instance, the quadrupolar mode associated with the oscillation of the aspect ratio of the cloud could be related to the formation of vortices in a BEC stirred by the rotation of an anisotropic harmonic potential [44]. The same quadrupolar mode was used to probe the angular momentum of a rotating condensate [45].

One specific mode, called the *scissor mode*, is more specifically connected to the issue of superfluidity. It is related to the reduction of the moment of inertia that is itself characteristic of a non classical fluid behaviour. In cold gases, the scissors mode is excited by the sudden tilting of one of the axes of an anisotropic trap (Fig. 4a). One can show that the quenching of the moment of inertia of the superfluid is associated with the existence of a single high frequency mode in the quadrupolar response of the cloud [46, 47]. By contrast, the response of a non condensed (i.e. non superfluid) Bose gas is characterized by two frequencies, one of them being proportional to the anisotropy of the trap, and therefore vanishingly small for weakly anisotropic potentials.The experimental observation of a single, high frequency scissor mode, hence proving superfluidity, was performed in Oxford by the group of C. J. Foot (Fig. 4b) [48, 49].

2.4   Probing superfluidity with a moving impurity

Apart from the measurement of the moment of inertia, another historical characterization of superfluidity in liquid helium is the absence of drag when an obstacle is moved along the superfluid below a certain critical velocity. A simple explanation of this property based on the structure of the excitation spectrum was proposed by Landau. He noted that when the perturbation imparted by the obstacle is small, the energy transfer due to the drag can be described by the formation of elementary excitations in the fluid. Using a simple energy-momentum balance, one can readily show that a viscous drag only happens when the relative velocity of the obstacle with respect to the superfluid is larger than the
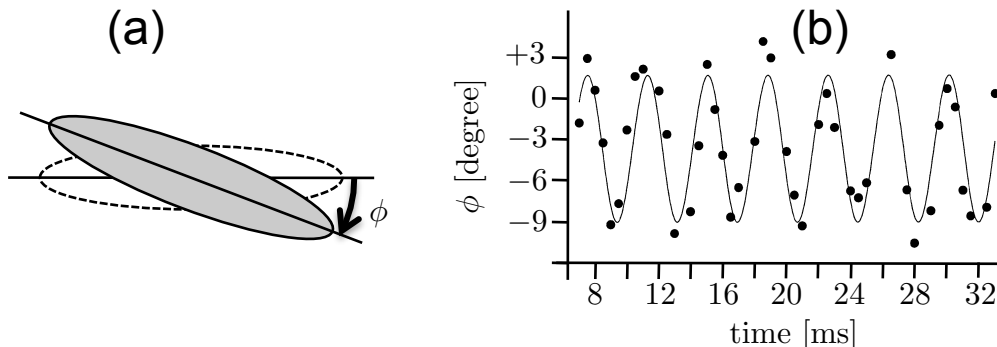
Figure 4: Scissors mode and superfluidity. (a) Schematic representation of the scissors mode: the axes of an anistropic trap are suddenly rotated by a small amount and one observes the subsequent dynamics of the cloud. (b) Oscillation of the condensate axis (scissors mode). Only one frequency appears in the oscillatory motion, which is a consequence of superfluidity (figure extracted from [48]).

critical velocity V_c given by the Landau criterion

$$V_c = \min_k \left(\frac{\omega_k}{k} \right) \ . \tag{20}$$

For the Bogoliubov spectrum (13), the critical velocity is simply the sound velocity. The drag can then be interpreted as an acoustic version of the Cerenkov radiation, associated in electromagnetism to the emission of an electromagnetic wake when a charged particle moves faster than the light velocity of the surrounding medium.

The absence of drag for a slowly moving microscopic impurity was tested quantitatively at MIT with a Sodium Bose–Einstein condensate. The impurities were also Sodium atoms that were transferred to an untrapped internal spin state using a stimulated Raman transition. In accordance with Landau's scenario, the scattering cross-section of the impurity with the condensed atoms dramatically decreased when the velocity of the impurity atom was smaller than the sound velocity in the BEC [50].

When the obstacle creating the perturbation has a larger size, the viscous drag is still negligible below a certain critical velocity, but the mechanism for the energy transfer is different. In this case, vortex shedding in the wake of the obstacle is the main source of dissipation in the system [51]. The onset of macroscopic dissipation was also studied by the group of W. Ketterle at MIT [52, 53]. They demonstrated that when a blue detuned laser creating a hole inside the condensate was moved, heating was observed only above a certain critical velocity (Fig.5). Using matter wave interferometric technics, superfluidity breakdown mechanism was latter on attributed to the nucleation of a vortex wake, in agreement with the large object scenario [54].

2.5 The case of long range forces: dipolar condensates

In some sense, the physics of dilute Bose–Einstein condensates with short range interactions constitutes an extension of the phenomena observed in liquid helium to the weak
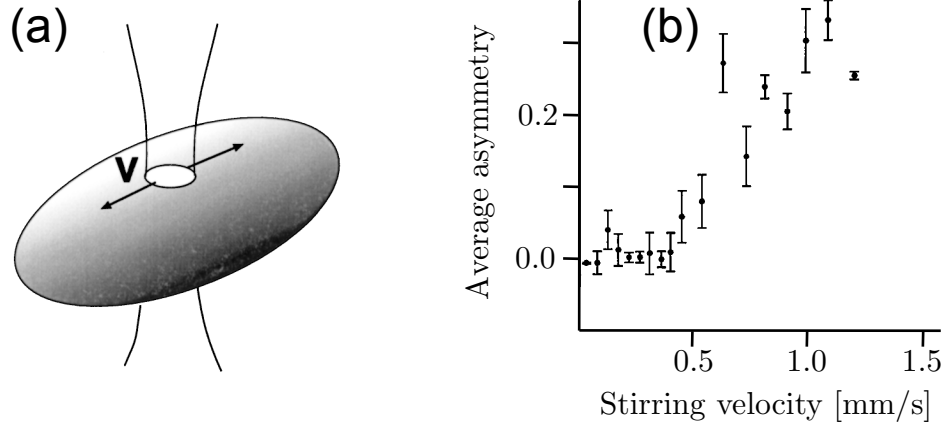
Figure 5: (a) Probing superfluidity: a blue detuned laser creating a repulsive potential is moved at constant velocity along a Bose–Einstein condensate (figure from [52]). (b) Drag force on the condensate, derived as an asymmetry in the density profile. The central sound velocity is $4.8\,\text{mm/s}$ (data from ref. [53]).

interaction regime $na_{\text{s}}^3 \ll 1$. By contrast, novel phenomena are expected when long range forces, like dipole-dipole interactions, are dominant. This explains why in recent years, much attention has been devoted to the realization of polar Bose–Einstein condensates [55].

At present, Bose–Einstein condensation of Chromium is the only successful attempt in this direction [56, 57]. Chromium is an atom with a rather large magnetic moment (six times that of an alkali) for which the ratio between long range and short range interactions can be modified using a Feshbach resonance. It is thus possible to achieve a situation where interactions are dominated by dipolar effects, in which case dramatic phenomena can be observed [55]. In addition to their long range character, dipolar forces are strongly anisotropic and their attractive or repulsive overall nature will depend on the geometry of the trapping potential. For cigare-shaped potentials and a dipole aligned with the trap axis, dipole forces are essentially attractive. In a pancake geometry and a dipole orientation perpendicular to the plane of the condensate, dipole forces are repulsive. In the first case, the cloud collapses due to an instability akin to the Rosensweig instability in classical ferrofluids [58]. By contrast, the repulsive interactions in a pancake geometry can overcome the instability of a Bose–Einstein with short range attractive interactions, as observed in [59].

In parallel with attempts to manipulate atomic species with larger magnetic moments (Erbium, Dysprosium [60]), other lines of research are currently exploring the possibility to produce quantum gases with electric dipole interactions, which exceed magnetic interaction by several orders of magnitude. One possibility is to take advantage of the large electric dipole moment that can exist for Rydberg atoms, i.e. atoms where one electron is excited to a high energy level [61]. Another promising option aims at producing a cold gas of heteronuclear molecules, using for example the photo-association of a mixture of two atomic gases [62, 63, 64].

3 Probing a condensate: the quantum approach

With the possibility to manipulate the confining potential in space and time, original probing schemes have been developed for atomic gases. Using interference experiments one can access the phase distribution of the fluid and its one-body distribution function. One can also measure the spatial distribution of particles in the gas with a single-atom resolution, and determine the density-density correlation function. In this section we present these probing schemes and illustrate them with some spectacular examples, such as the interference between independent condensates, the beat between two atom lasers, and the atomic Hanbury Brown and Twiss effect.

3.1 Interference of condensates

The prime feature of Bose–Einstein condensation is the accumulation of many particles in a single quantum state. It is reminiscent of laser operation principle, where a macroscopic number of photons accumulate in the same mode of an electomagnetic cavity. The first probe that we describe here is a direct proof of this macroscopic population of a single level.

We start with an experiment that W. Ketterle and his group performed in 1997 [15]. It constituted an experimental answer to a question raised by P.W. Anderson [65]:"Do two superfluids that have never seen one another possess a definite relative phase?". The center of a magnetic trap was irradiated by a light sheet creating a large repulsive barrier to produce a double well potential (figure 6a). Using evaporative cooling a condensate was prepared around each potential minimum. Then the magnetic trap was switched off as well as the light sheet. The two atom clouds expanded and overlapped, and an image of the resulting spatial distribution was taken. The density profile exhibited interference fringes with a large contrast ($> 70\%$), which proved the coherence of each initial cloud (figure 6b).

To give a quantitative account for the interference pattern, the simplest approach consists in associating a classical field with a random phase φ_j ($j = 1, 2$) to each condensate [66]. Here we assume that the condensates are centered on the points $\pm \boldsymbol{a}/2$ and we neglect for simplicity the role of atomic interaction during the time-of-flight (TOF) expansion. This approximation may be questionable for short expansion times t, but becomes eventually correct since the atomic density drops as t^{-3} when t increases. The expansion of each condensate wave function is thus obtained using the single-particle propagator associated with the Schrödinger equation. Assuming that the initial distance a between the condensates is much larger than their initial size, the density at a point $\boldsymbol{r}$ after a TOF duration t is approximately proportional to

$$
\begin{aligned}
\rho(\boldsymbol{r}, t) \quad &\propto \quad \left| \exp\left[\varphi_1 + im(\boldsymbol{r} + \boldsymbol{a}/2)^2/2\hbar t\right] + \exp\left[\varphi_2 + im(\boldsymbol{r} - \boldsymbol{a}/2)^2/2\hbar t\right] \right|^2 \\
&\propto \quad \cos^2(\Delta\varphi + m\boldsymbol{r} \cdot \boldsymbol{a}/2\hbar t) ,
\end{aligned}
\tag{21}
$$

where $\Delta\varphi = \varphi_1 - \varphi_2$. The interference pattern consists of straight fringes perpendicular to the line joining the condensate centers, with a fringe spacing equal to ht/ma. The contrast of the interference reaches 100% in this simple model, as a result of the macroscopic
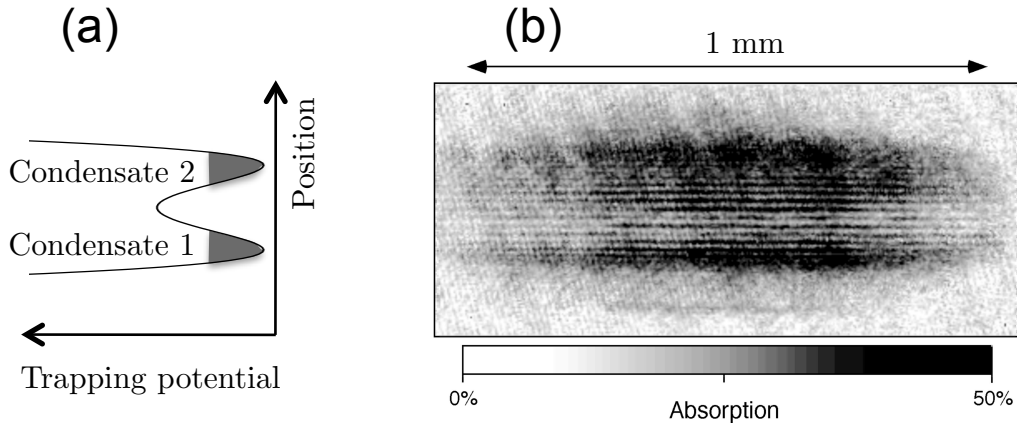
Figure 6: (a) Double well potential obtained by shining the center of the magnetic trap with a laser beam. After evaporation one obtains two independent condensates. (b) After release from the magnetic+optical potential the two condensates expand and overlap. The spatial distribution in the overlap region shows interference fringes with a large contrast (photograph: courtesy of W. Ketterle, MIT).

occupation of a single quantum state. For a given experimental shot, the positions of the bright fringes give access to the relative phase $\Delta\varphi$ between the two condensates. The relative phase fluctuates randomly from shot to shot, and the superposition of many interference patterns recorded in the same experimental condition leads to a uniformly grey image.

One can also explain the emergence of the interference pattern by assuming that the initial state of the two condensates is of the form $|N_1, N_2\rangle$, with a well defined number of particles N_1 and N_2 in each subsystem. In this case the phases φ_1 and φ_2 are initially not defined and the probability distribution for the relative phase $\varphi_1 - \varphi_2$ is a uniform function between 0 and 2π. The phase distribution evolves towards a narrower distribution as the number of detected atoms increases. In this point of view the emergence of a relative phase is a consequence of the information acquired on the system via the atomic position measurements [67, 68, 69]. Such interfering independent condensates can be used to investigate possible violations of local realism, using generalized Bell-type inequalities [70].

So far we restricted our discussion to the case of independent condensates, assuming that the tunneling between the central barrier was negligible on the time scale of the experiment. When the coupling between the two sides of the barrier is significant, the situation is reminiscent of a Josephson junction and it can give rise to a wealth of quantum phenomena such as quantum self trapping [71] and a.c./d.c. Josephson effects [72]. Repulsive interactions between particles in this double well geometry can also lead to a reduction of the fluctuations of $N_1 - N_2$. This so-called *number squeezing* was demonstrated in [73] and can lead to a significant improvement of atom interferometry methods [74, 75].

3.2 One-body correlation function

The most direct tool to investigate the formation of a Bose–Einstein condensate is the one-body correlation function

$$G_1(\boldsymbol{r}, \boldsymbol{r}') = \langle \hat{\psi}^\dagger(\boldsymbol{r}) \hat{\psi}(\boldsymbol{r}') \rangle , \tag{22}$$

where the operator $\hat{\psi}^\dagger(\boldsymbol{r})$ creates a particle in $\boldsymbol{r}$. For a uniform fluid, G_1 depends only on the distance $|\boldsymbol{r} - \boldsymbol{r}'|$ and the Penrose–Onsager criterion relates Bose–Einstein condensation with a non-zero limit of G_1 when $|\boldsymbol{r} - \boldsymbol{r}'|$ tends to infinity [76]. For a non-degenerate ideal atomic gas, G_1 is a gaussian function that decays to zero over a distance of the order of the thermal wavelength λ.

Several strategies have been developed to access G_1. One can take advantage of the fact that the momentum distribution $\mathcal{P}(\boldsymbol{p})$, which can be measured using the Bragg spectroscopy method presented in the previous section, is the Fourier transform with respect to the variable $\boldsymbol{u}$ of $\int G_1(\boldsymbol{R} + \boldsymbol{u}/2, \boldsymbol{R} - \boldsymbol{u}/2) \, dR$. Here we rather concentrate on a direct measurement of G_1, which can be obtained by looking at the interference of one part of the gas located around $\boldsymbol{r}$ with another part located around $\boldsymbol{r}'$.

The NIST group developed a procedure that consists in measuring the interference between two spatially displaced copies of an original condensate [77]. In the NIST experiment each copy was produced using a light pulse with a laser standing wave along a given direction z, which transferred a small fraction of the atoms of the BEC to a state with momentum $\boldsymbol{p}_0 = 2\hbar k \hat{\boldsymbol{z}}$, where k is the wave vector of the photons and where $\hat{\boldsymbol{z}}$ is a unit vector along the z axis. This momentum kick $\boldsymbol{p}_0$ resulted from the absorption of a photon in one of the beams creating the standing wave, and from the stimulated emission of a photon in the other beam. The kick p_0 was much larger than the typical momentum of an atom in the trapped BEC. The total number of atoms with momentum p_0 was measured as a function of the time t between the two light pulses. For a pure condensate one can show that this number is related to the overlap between the initial condensate wave function and the same wave function displaced by a distance $\boldsymbol{\rho} = \boldsymbol{p}_0 t/m$. More generally this method gives access to the integral over $\boldsymbol{r}$ of $G_1(\boldsymbol{r}, \boldsymbol{r} + \boldsymbol{\rho})$. It has been used by several groups to study the emergence of coherence in atomic gases in particular in low dimension systems.

A second procedure consists in generating two continuous atomic beams out of an atom cloud, and in looking at the spatial interference between these beams. We show in figure 7 a result obtained by the Munich group. The atoms were confined in a magnetic trap and each beam was extracted using a radio-frequency (rf) electromagnetic field. As for evaporative cooling (see § 1.4), the rf flipped the magnetic moments of the atoms at some definite locations. After the flip these atoms were not trapped anymore and felt under the influence of gravity. The choice of the rf value determined the precise location in the trap from which the atoms were extracted [78]. When a single rf wave is applied, the atomic beam produced in this way is often refered to as an *atom laser* [79]. By applying simultaneously two different rf values, the Munich group obtained two atomic beams emerging from two different points of the atom cloud (see fig. 7a) [16]. When the temperature T was chosen well below the critical temperature T_c for BEC, they observed an interference with a large contrast in the region where the two atomic beams overlapped
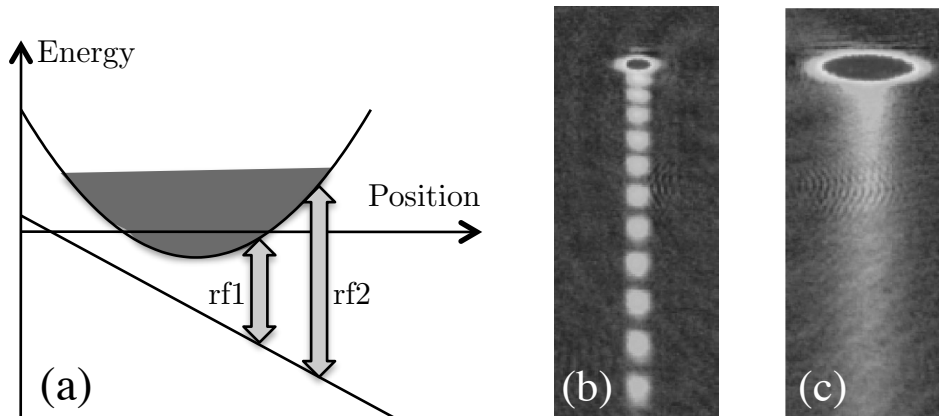
Figure 7: *(a) Extraction of two atomic beams (“atom lasers”) from a cloud of rubidium atoms. Two radio-frequency waves, rf1 and rf2, flip the magnetic moment of the atoms at well defined positions in the trap. After the spin flip the atoms are in an internal state that is not confined in the magnetic trap, and they fall under gravity. (b) The atom cloud is a quasi-pure condensate and a strong interference contrast is observed between the two beams, which reveals the phase coherence of the sample. (c) For a cloud above the critical temperature, no phase coherence is measured if the distance between the extraction points exceeds 200 nm (photographs: courtesy of Immanuel Bloch, Munich).*

(fig. 7b). The interference pattern remained visible even for a large difference between the two radio-frequencies, corresponding to a distance between the two point sources of the order of the size of the cloud. On the opposite when $T > T_c$, no detectable interference was visible in the zone where the two beams overlap (fig. 7c), unless the distance between the two sources was below 200 nm, i.e. the coherence length of the gas $\ell \approx \lambda$ in these experimental conditions. The measurement of the visibility of the interference pattern between two matter-waves also provides a mean to investigate the critical behaviour of the gas at the Bose–Einstein condensation point [80].

3.3 Two-body correlation function and Hanbury Brown and Twiss effect

In general the one-body correlation function does not capture all the physics of a many-body system and one needs correlation functions involving an arbitrary number of particles to characterise fully the state of a quantum fluid. The measurement of the two-body correlation function

$$G_2(\boldsymbol{r}, \boldsymbol{r}') = \langle \hat{\psi}^\dagger(\boldsymbol{r})\, \hat{\psi}^\dagger(\boldsymbol{r}')\, \hat{\psi}(\boldsymbol{r}')\hat{\psi}(\boldsymbol{r}) \rangle \tag{23}$$

is a particularly important step. Indeed G_2 corresponds to the probability to detect one atom in $\boldsymbol{r}$ and another atom in $\boldsymbol{r}'$, and it gives access to the density fluctuations in the superfluid, by contrast to G_1 that characterizes its phase fluctuations.

An efficient tool to measure G_2 is a position-resolved single atom counter. Here we briefly describe results obtained in a collaboration between the Amsterdam and Orsay groups, using a microchannel plate to detect metastable Helium atoms [81, 82]. The plate

was placed below the atom cloud; when released from the trap, the atoms felt on the plate and the position of each detected atom in the horizontal plane was recorded, as well as its arrival time. Assuming ballistic expansion one could then reconstruct the *in situ* G_2 function. This experiment provided a nice illustration of the Hanbury Brown and Twiss (HBT) effect, i.e. the bunching of bosonic particles in a thermal source, corresponding to a maximum of G_2 for $\boldsymbol{r} = \boldsymbol{r}'$. The HBT effect can be interpreted in simple terms, by considering the detection in $\boldsymbol{r}$ and $\boldsymbol{r}'$ of two atoms that were in different initial states a and b. There are two quantum paths $\{a \to \boldsymbol{r}, b \to \boldsymbol{r}'\}$ and $\{a \to \boldsymbol{r}', b \to \boldsymbol{r}\}$ that correspond to this process and that can interfere. For bosonic particles, thanks to the symmetry of the global wave function by exchange of the two particles, the interference is constructive in $\boldsymbol{r} = \boldsymbol{r}'$ and provides the HBT bunching. For thermal Bose gases the observation of this bunching was reported in [83, 81]. The bunching is not present for a pure condensate, because all particles then occupy the same initial state [81]. If the experiment is performed with a Fermi gas instead of a Bose gas (^{3}He instead of ^{4}He for example), one expects from Pauli principle an antibunching of particles at $\boldsymbol{r} = \boldsymbol{r}'$. This was indeed observed in [82].

A technique that is also directly inspired from the HBT effect is quantum noise interferometry [84]. This method, which does not require a detection at the single atom level, is based on the autocorrelation function of individual images of a quantum gas. Many images are taken in the same experimental conditions (temperature, chemical potential), and each image differs from the others only in its atomic shot noise. The average of the auto-correlation function over these many images provides the desired density-density correlation function. Spectacular illustrations of this technique are the evidence for the spatial order of the Mott-insulator state of a gas in an optical lattice [85], and the detection of correlations between pairs of atoms produced in the dissociation of a weakly bound molecule [86].

Finally let us mention that one can access higher order correlation functions (at least their values at short distances) by looking at the loss rate from the gas. As mentioned above, the main loss process in cold atomic gases is usually three-body recombination. This process occurs when three atoms are close to each other; two of them can form a dimer bound state, and the third atom carries away the released energy. The corresponding rate is approximately proportional to $\langle n^3(\boldsymbol{r}) \rangle$, and its measurement as a function of temperature and density allows one to follow the entrance of the gas in the quantum degenerate regime [87]. In particular for a constant density $\langle n \rangle$, one can observe the reduction of $\langle n^3 \rangle$ by a factor $3! = 6$ between a thermal state and a pure condensate [88]. The strong decrease of the three-body recombination rate in a quasi-one dimensional gas was also used as a signature of the entrance in the strongly correlated Tonks-Girardeau regime [89].

4 Low dimensional aspects: BEC vs. superfluidity

Dimensionality has a strong influence on the type of phase transitions that can take place in a physical system [90]. Indeed, phase transitions result from a competition between cooperativity effects and quantum or thermal fluctuations. Because a particle in a 1d

or 2d geometry has less neighbours than in 3d, the role of interactions is weakened and disordered states are favored. More precisely, the Mermin-Wagner theorem states that long range order cannot occur at non-zero temperature in a 1d or 2d system with short-ranged interactions and a continuous symmetry [91]. An illustration of this result is the absence of Bose–Einstein condensation in an infinite, homogeneous Bose gas in one or two dimensions [92], which holds both for the ideal and interacting cases.

The absence of true Bose–Einstein condensation in a low-dimensional gas is still compatible with the presence of a superfluid component. The proper definition of superfluidity is based on the sensitivity of the N-body wave function $\Psi(\boldsymbol{r}_1, \ldots, \boldsymbol{r}_N)$ with respect to a boost modeled by a change in the boundary conditions. Instead of choosing the usual periodic boundary conditions in a box of size L, one can consider twisted boundary conditions such that Ψ is multiplied by $e^{i\theta}$ when the coordinates $\boldsymbol{r}_i$ are increased by $L\boldsymbol{e}$, where $\boldsymbol{e}$ is a unit vector along one of the directions of space. If the system is normal (non superfluid) its free energy is unaffected by the phase twist. On the contrary a superfluid system possesses some phase rigidity, and its free energy increases by an amount ΔF proportional to θ^2 for small θ. The rigourous definition of the superfluid density is then based on the non-zero value of the ratio $\Delta F/\theta^2$. From a practical point of view the twist in the boundary conditions is provided by a slow rotation of the system, and the angle θ is the Sagnac phase appearing in the frame rotating with the gas. The non-zero value of ΔF corresponds to a reduction of the moment of inertia of the gas, with respect to the value expected for a classical fluid. Twisted boundary conditions can also be imposed by taking advantage of the geometric Berry's phase [93].

In the following we discuss the case of the superfluid transition in a two-dimensional Bose gas. We first recall why no Bose–Einstein condensation occurs in an infinite, ideal gas, and we briefly describe the Berezinski–Kosterlitz–Thouless mechanism that is at the origin of the superfluid transition in this system. We then turn to trapped two-dimensional atomic gases, for which the finite-size of the system makes possible the emergence of a significant condensed fraction at a non-zero temperature. To keep this section within a reasonable length, we do not address here the case of the superfluidity of one-dimensional systems and we refer the reader to [94] and refs. in for a discussion of this problem.

4.1   The superfluid transition in a uniform 2d gas

For an ideal 2d gas, the absence of Bose–Einstein condensation at any non-zero temperature is a direct consequence of the equation of state

$$n_2\lambda^2 = -\ln(1-Z) \ , \tag{24}$$

where n_2 is the surface density of the gas and Z the fugacity defined as $Z = \exp(\mu/k_{\mathrm{B}}T)$. From this result it is clear that one can associate a value of the chemical potential to an arbitrary large phase space density $n_2\lambda^2$. This is very different from the 3d situation where, as mentioned in the first section, the equation of state for the ideal gas no longer possess any solution for $n_3\lambda^3 > \zeta(3/2)$.

The two-dimensional situation is marginal in the sense that although thermal fluctuations prevent the apparition of a true Bose–Einstein condensate, a superfluid transition

at a non-zero temperature is still possible. This transition has been investigated with a great precision in helium films [95]. Its key feature, first described by Berezinskii [96] and by Kosterlitz and Thouless [97] (BKT), is well captured by the decay at large distances $|\boldsymbol{r} - \boldsymbol{r}'|$ of the one-body correlation function $G_1(\boldsymbol{r} - \boldsymbol{r}')$ defined in (22). For a Bose gas with repulsive interactions, three regimes can be identified when the temperature is decreased while maintaining a fixed spatial density n_2. At high temperature, the interaction energy is negligible compared to $k_{\mathrm{B}}T$; in this case G_1 is a gaussian function that tends to zero over a distance given by the thermal wavelength λ. When T is lowered, the interaction energy becomes significant and density fluctuations are gradually suppressed. The decay of G_1 then becomes exponential with a characteristic length ℓ that increases when the temperature decreases. At a critical temperature T_{c}, the length ℓ diverges and a fraction of the gas becomes superfluid. For $T < T_{\mathrm{c}}$, the one-body correlation function still decays at infinity (otherwise a true BEC would be present) but the decay is only algebraic: $G_1 \propto |\boldsymbol{r} - \boldsymbol{r}'|^{-\alpha}$. Remarkably the 2d superfluid density $n_{2,\mathrm{s}}$ is related to the exponent α by the simple law $\alpha = 1/n_{2,\mathrm{s}}\lambda^2$. Just below T_{c}, the exponent α takes the universal value $1/4$ irrespective of the strength of the interactions, so that $n_{2,\mathrm{s}}^{(\mathrm{c})} = 4/\lambda^2$ [98]. Note that the universal relation $n_{2,\mathrm{s}}^{(\mathrm{c})}\lambda^2 = 4$ giving the critical point is implicit, since $n_{2,\mathrm{s}}$ is itself a function of temperature. The relation between the total density n_2 and the temperature at the critical point has been determined numerically in [99] in the regime of weak interactions. It can be written

$$n_2^{(\mathrm{c})}\lambda^2 = \ln(C/g) \; , \tag{25}$$

where $g \ll 1$ is the dimensionless parameter characterising the interactions in the 2d fluid and $C \approx 380$ is a constant.

The microscopic mechanism at the origin of the 2d superfluid transition is the breaking of vortex pairs. In this context a vortex is a point in space where the superfluid density vanishes, and around which the phase rotates by $\pm 2\pi$ (vortices corresponding to multiples of $\pm 2\pi$ play a negligible role in practice). In the domain of temperature of interest, the relevant excitations of the fluid are either vortices or phonons, both corresponding to phase fluctuations. Density fluctuations play a minor role at least at the qualitative level. In the low temperature superfluid phase, vortices can only exist in the form of bound pairs, formed by the association of two vortices with opposite circulation. Indeed the free-energy cost of a single isolated vortex is large and even diverges in the thermodynamic limit. When the temperature increases and $n_{2,\mathrm{s}}\lambda^2$ reaches the value 4, the free energy for a single vortex decreases and finally vanishes. Isolated vortices can then appear, which further reduces the value of $n_{2,\mathrm{s}}$ and makes the emergence of other free vortices even more likely. This avalanche effect entails that the properly renormalized superfluid density vanishes [97, 98].

4.2   The 2d trapped Bose gas

Cold atom experiments are usually performed in a harmonic potential and the confinement modifies significantly the results obtained for the infinite homogeneous case. We consider first an ideal gas in an isotropic potential of frequency ω. The single particle density of states is proportional to the energy, like for a particle moving freely in a 3d space. One

recovers therefore a genuine Bose–Einstein condensation when the number of particles exceeds the critical number [100]

$$N_{\rm c} = \frac{\pi^2}{6} \left(\frac{k_{\rm B} T}{\hbar \omega} \right)^2 . \tag{26}$$

This transition survives in the thermodynamic limit, which corresponds for a two-dimensional harmonic trap to letting the number of particles N go to infinity, the trap frequency ω go to 0, while keeping the product $N\omega^2$ constant.

The next question is whether this result still holds in presence of interactions. The answer is quite subtle (see [101] for a review) and we outline here only the main results. The simplest approach is based on the mean-field Hartree-Fock approximation, in which repulsive interactions are accounted for by adding a term proportional to the density $n_2(\boldsymbol{r})$ to the trapping potential. The mean-field energy reduces the strength of the confinement at the bottom of the trap, where the density is the largest, and makes the situation very similar to the case of a 2d gas in a flat potential. A quantitative analysis shows that this flattening of the confinement has a dramatic effect: within the mean-field description, the singularity for $N > N_{\rm c}$ that was signalling the condensation for an ideal gas disappears [102].

The Hartree-Fock approach is however not the end of the story. Indeed it does not predict the superfluid BKT transition when it is applied to the uniform infinite system. To go further it is convenient to turn to the local density approximation, and make use of the known results for the infinite uniform 2d gas [103]. Within this approximation one predicts that the superfluid transition takes place in the trapped system when the phase space density at the center of the trap reaches the critical value (25). This approximation has been accurately checked by a Quantum Monte Carlo calculation [104] as well as with semi-classical field simulations [105].

Let us now focus on the case where a superfluid with a size L has formed at the bottom of the trap. Is there also a significant condensed fraction in this case? We recall that the answer would be negative in an infinite uniform system, because the one-body correlation function G_1 decays algebraically with distance in a low temperature two-dimensional gas. However for a system of finite size L this argument does not apply. The condensed fraction f, which is defined as the largest eigenvalue of the one-body density operator, is approximately given in this case by $G_1(L) \sim (\xi/L)^\alpha$, where ξ is the healing length. We mentioned above that the exponent α is smaller than $1/4$; taking as a typical value $L \sim 100\,\xi$ we find $f \geq 0.3$, which is confirmed by Monte Carlo calculations [104, 106]. We reach here a conclusion that is well known in the domain of two-dimensional magnetism [107]: Because of finite size effects, the two phenomena of superfluidity and condensation cannot be dissociated for any practical case.

4.3   Making a 2d atomic fluid in practice

In order to realise experimentally a 2d atomic gas in the xy plane, one usually freezes the third degree of freedom with a laser beam that provides a strong confinement $m\omega_z^2 z^2/2$ along the z direction. If the temperature and the chemical potential are both smaller

than $\hbar\omega_z$, the gas can be considered as a 2d system from the thermodynamic point of view, with a thickness given by the size of the ground state of the harmonic oscillator along z, $a_z = \sqrt{\hbar/m\omega_z}$. The 3d scattering length a_s is usually much smaller than a_z so that atom interactions can still be described by the usual 3d scattering formalism [108]. The interaction energy of the gas E_{int} can then be written in good approximation $E_{\text{int}} = (\hbar^2 g/2m) \int n_2^2(\boldsymbol{r}) \, d^2 r$, with $g = \sqrt{8\pi} a_s/a_z$.

The simplest laser scheme that produces the required confinement along z is a single gaussian beam. It must be red-detuned with respect to the atomic resonance, so that the atoms are attracted by the dipole force towards the high intensity region [109]. The beam is focused with a cylindrical lens in order to produce a horizontal light sheet with a thickness of a few microns. More elaborate schemes involve evanescent waves at the surface of a dielectric medium, optical lattices and holographic wave plates (see [94] for a review). The first diagnosis of a 2d gas consists in measuring its density profile in the xy plane, either *in situ* or after a time-of-flight. Experiments with rubidium atoms, corresponding to $g = 0.15$, have shown the existence of a sharp transition [110, 111]. For a small phase space density at center, the density profile is smooth and relatively well described by a single gaussian function. Above a critical value (which is in good agreement with the BKT prediction (25)), a narrow feature appears at the center of the trap on the top of a broader distribution, in good agreement with a two-fluid model. For experiments performed with sodium, a good description of the data around the critical point is obtained only if one introduces a third intermediate component, which is interpreted as a "non-superfluid" quasi-condensate [112]. A possible hint to explain the differences between the sodium and rubidium cases is the notably smaller interaction parameter for the Na experiment ($g = 0.02$), making it closer to the ideal gas case.

Further insight on 2d gases is provided by the measurement of the function G_1, which characterises the phase distribution in the fluid. In order to access it, one can interfere two independent planes of atoms prepared in the same conditions (fig. 8a) and study the distribution of contrasts of the interference patterns [113, 114]. Such a measurement was performed with rubidium atoms and gave evidence for the rapid increase of coherence of the gas below the critical point (figs. 8b-d) [115]. In addition some interference patterns revealed the presence of isolated vortices, which appear as dislocations of the fringe system (fig. 8d). The number of dislocations increased with temperature, until the critical point was reached and the interference disappeared. The link between fringe dislocations and vortices was confirmed by numerical simulations based on a classical field stochastic evolution [116]. Another way for measuring G_1 is a homodyning method, in which one interferes the 2d gas with its own copy, after it has been displaced by an adjustable distance [112]. This method is reminiscent of the one presented in § 3.2 for 3d samples, and it gives access to the coherence length ℓ of the gas as a function of temperature above and below the critical point. The authors of [112] could observe in this way the transition between the 'hot' regime where $\ell \sim \lambda$ and the colder one where $\ell \gg \lambda$.

The research on 2d atomic superfluids is still a very open field of research and many issues remain to be investigated. We will mention here only two of them. The first series of problems deals with 'out of equilibrium' questions: how do two independent planes dephase with respect to each other, if their phases were locked at initial time? This question has already been experimentally answered for 1d gases [117] and it would be
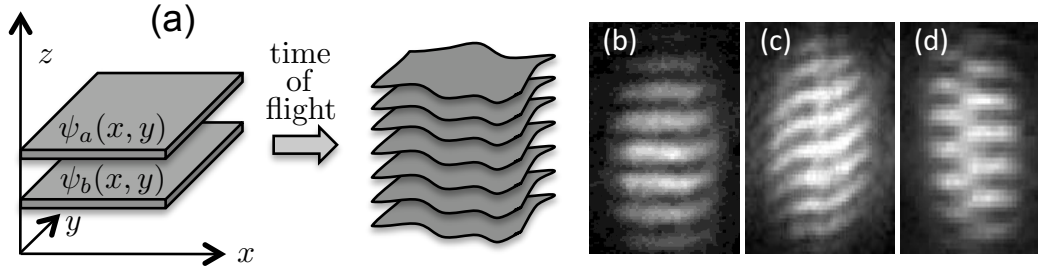
Figure 8: (a) Interference between two independent planar gases, observed after time-of-flight. (b-d): Examples of interference patterns measured with the experimental setup described in [115]. The imaging beam is propagating along the y axis. The pattern (b) is obtained with very cold gases, whereas (c) corresponds to a larger temperature. The dislocation in (d) is the signature for the presence of a vortex in one of the two gases.

interesting to revisit it for 2d fluids, where the loss of coherence is predicted to behave as a power-law function of the evolution time [118]. A second crucial aspect is the direct determination of the superfluid component, by measuring for example the moment of inertia of the gas. Up to now, investigations on 2d fluids have mostly focused on phase coherence. Looking directly at superfluid properties would allow one to draw a bridge with the physics of helium films, where transport measurement is a natural diagnostic [95].

5 Summary and Outlook

We presented in this Chapter the methods that allow one to prepare and probe a quantum atomic gas. These gases provide a practical realisation of a paradigm of many-body theory: the weakly interacting Bose gas. This model was developed in the period 1950-70 but could not be applied in a quantitative manner to the only Bose superfluid (liquid ^{4}He) that existed at that time. Indeed in superfluid ^{4}He the interactions are strong and lead to a severe depletion of the condensate even at zero temperature. On the contrary the interparticle distance in atomic gases is usually much larger than the scattering length characterising the interactions, and the microscopic description of the fluid in terms of the Gross–Pitaevskii equation (GPE) is an excellent approximation. The Bogoliubov linearisation of the GPE provides an excitation spectrum that is in very good agreement with experimental observations, and the GPE can even be used to study the turbulent dynamics of theses gases ([119] and the Chapter by M. Tsubota, K. Kasamatsu, and M. Kobayashi in the present book).

By contrast to 'conventional' superfluids like liquid ^{4}He or superconductors, transport measurements are not well suited for atomic vapours. The required 'circuitry' would be in most cases difficult to implement with the standard tools of atomic physics: magnetic fields and laser beams. Therefore the investigation of atomic gases required the development of novel probing techniques: time-of-flight expansion, Bragg spectroscopy, interference between independent samples, etc.. These tools give access in particular to the momentum

distribution of the particles or to its Fourier transform, the one-body correlation function G_1. Recently the achievement of detection methods at the single atom level (see e.g. [120]) open the opportunity to take a direct 'snapshot' of a many-body wave function.

The possibilities opened by the achievement of degenerate atomic gases go well beyond the mean-field physics described by the GPE. A celebrated example is the transition from superfluid to Mott-insulator states, which can be observed with a gas confined in an optical lattice (see [121] and the Chapter by Tin-Lun Ho in this book). Another class of strongly correlated states that are actively looked for, are the analogues of those appearing in fractional Quantum Hall effect. Such states are expected to emerge in an atomic gas submitted to a strong gauge field [122]. This gauge field can originate from a fast rotation of the system, or from the geometrical phase accumulated by an atom when it follows adiabatically one of its internal states [94]. The study of the BEC-BCS cross-over also belongs to 'beyond mean-field' physics, using fermionic species instead of bosonic ones (see the Chapter by M. Zwierlein).

To keep this Chapter within reasonable length we had to omit several important developments of many-body physics with cold atomic gases. We restricted in particular to single components superfluids, but we should mention that the research on multi-component gases is also very active. One can take advantage of the spin degeneracy and prepare a spinor gas with 3 (5) components for a $F = 1$ (2) atomic state, which leads for example to a spectacular texture dynamics [123]. One can also mix two different atomic species (or even three species like in [124]) with different masses and possibly different statistical nature (Bose-Bose, Bose-Fermi and Fermi-Fermi). Finally we mention a promising emerging subject, devoted to the effect of disorder on superfluidity. Recent experiments studied the localisation of atoms in a disordered potential created by laser light in a one-dimensional geometry [125, 126]. The transition to two and three dimensions is now underway [127], and these studies could help clarifying the subtle interplay between single-particle Anderson localization phenomenon and superfluidity of an interacting gas.

References

[1] P. Kapitza. Viscosity of liquid helium below the λ-point. *Nature*, 141:74, 1938.

[2] J. F. Allen and A. D. Misener. Flow of liquid helium II. *Nature*, 141:75, 1938.

[3] A. Einstein. Quantentheorie des einatomigen idealen gases. *Sitzungsberichte/Physikalische Klasse, Preussische Akademie der Wissenschaften*, 22:261, 1924.

[4] A. Einstein. Quantentheorie des einatomigen idealen gases. ii. *Sitzungsberichte/Physikalische Klasse, Preussische Akademie der Wissenschaften*, 1:3, 1925.

[5] Peter Grüter, David Ceperley, and Frank Laloë. Critical temperature of bose-einstein condensation of hard-sphere gases. *Phys. Rev. Lett.*, 79(19):3549–3552, Nov 1997.

[6] M. H. Anderson, J. R. Ensher, M. R. Matthews, C. E. Wieman, and E. A. Cornell. Observation of Bose–Einstein condensation in a dilute atomic vapor. *Science*, 269:198, 1995.

[7] K. B. Davis, M.-O. Mewes, M. R. Andrews, N. J. van Druten, D. S. Durfee, D. M. Kurn, and W. Ketterle. Bose–Einstein condensation in a gas of Sodium atoms. *Phys. Rev. Lett.*, 75:3969, 1995.

[8] C. C. Bradley, C. A. Sackett, and R. G. Hulet. Bose–Einstein condensation of lithium: Observation of limited condensate number. *Phys. Rev. Lett.*, 78:985, 1997.

[9] M. Greiner, C. A. Regal, and D. S. Jin. Emergence of a molecular Bose–Einstein condensate from a fermi gas. *Nature*, 426:537, 2003.

[10] S. Jochim, M. Bartenstein, A. Altmeyer, G. Hendl, S. Riedl, C. Chin, J. Hecker-Denschlag, and R. Grimm. Bose–Einstein condensation of molecules. *Science*, 302:2101, 2003.

[11] M. W. Zwierlein, C. A. Stan, C. H. Schunk, S. M. F. Raupach, S. Gupta, Z. Hadzibabic, and W. Ketterle. Observation of Bose–Einstein condensation of molecules. *Phys. Rev. Lett.*, 91:250401, 2003.

[12] A. J. Leggett. Bose–Einstein condensation in the alkali gases. *Rev. Mod. Phys.*, 73:333, 2001.

[13] L. Pitaevskii and S. Stringari. *Bose–Einstein Condensation*. Oxford University Press, Oxford, 2003.

[14] C.J. Pethick and H. Smith. *Bose–Einstein Condensation in Dilute Gases*. Cambridge University Press, 2002.

[15] M. R. Andrews, C. G. Townsend, H. J. Miesner, D. S. Durfee, D. M. Kurn, and W. Ketterle. Observation of interference between two Bose condensates. *Science*, 275:637, 1997.

[16] I. Bloch, T. W. Hänsch, and T. Esslinger. Measurement of the spatial coherence of a trapped Bose gas at the phase transition. *Nature*, 403:166, 2000.

[17] S. Chu. Nobel Lecture: The manipulation of neutral particles. *Rev. Mod. Phys.*, 70:685, 1998.

[18] C. Cohen-Tannoudji. Nobel Lecture: Manipulating atoms with photons. *Rev. Mod. Phys.*, 70:707, 1998.

[19] W.D. Phillips. Nobel Lecture: Laser cooling and trapping of neutral atoms. *Rev. Mod. Phys.*, 70:721, 1998.

[20] E. L. Raab, M. Prentiss, A. Cable, S. Chu, and D. E. Pritchard. Trapping of neutral sodium with radiation pressure. *Phys. Rev. Lett.*, 59:2631, 1987.

[21] K. Huang. *Statistical Mechanics*. Wiley, New-York, 1987.

[22] H. Katori, T. Ido, Y. Isoya, and M. Kuwata-Gonokami. Magneto-optical trapping and cooling of Strontium atoms down to the photon recoil temperature. *Phys. Rev. Lett.*, 82:116, 1999.

[23] T. Kuwamoto, K. Honda, Y. Takahashi, and T. Yabuzaki. Magneto-optical trapping of Yb atoms using an intercombination transition. *Phys. Rev. A*, 60:745–748, 1999.

[24] C. G. Townsend, N. H. Edwards, C. J. Cooper, K. P. Zetie, C. J. Foot, A. M. Steane, P. Szriftgiser, H. Perrin, and J. Dalibard. Phase-space density in the magneto-optical trap. *Phys. Rev. A*, 52:1423, 1995.

[25] R. Grimm, M. Weidemüller, and Y. B. Ovchinnikov. Optical dipole traps for neutral atoms. *Adv. At. Mol. Opt. Phys.*, 42:95, 2000.

[26] O. J. Luiten, M. W. Reynolds, and J. T. M. Walraven. Kinetic theory of evaporative cooling of a trapped gas. *Phys. Rev. A*, 53:381, 1996.

[27] W. Ketterle and N. J. van Druten. Evaporative cooling of trapped atoms. In B. Bederson and H. Walther, editors, *Advances in Atomic, Molecular, and Optical Physics*, volume 37, pages 181–236. Academic Press, San Diego, 1996.

[28] E. A. Cornell and C. E. Wieman. Nobel Lecture: Bose–Einstein condensation in a dilute gas, the first 70 years and some recent experiments. *Rev. Mod. Phys.*, 74(3):875–893, 2002.

[29] W. Ketterle. Nobel lecture: When atoms behave as waves: Bose–Einstein condensation and the atom laser. *Rev. Mod. Phys.*, 74(4):1131–1151, 2002.

[30] M. D. Barrett, J. A. Sauer, and M. S. Chapman. All-optical formation of an atomic Bose–Einstein condensate. *Phys. Rev. Lett.*, 87(1):10404, 2001.

[31] F. S. Dalfovo, L. P. Pitaevkii, S. Stringari, and S. Giorgini. Theory of Bose–Einstein condensation in trapped gases. *Rev. Mod. Phys.*, 71:463, 1999.

[32] F. Gerbier, J. H. Thywissen, S. Richard, M. Hugbart, P. Bouyer, and A. Aspect. Critical temperature of a trapped, weakly interacting Bose gas. *Phys. Rev. Lett.*, 92(3):030405, 2004.

[33] E.P. Gross. Structure of a quantized vortex in Boson systems. *Il Nuovo Cimento*, 20(3):454–477, 1961.

[34] L. P. Pitaevskii. Vortex lines in an imperfect Bose gas. *Sov. Phys. JETP*, 13(2):451–454, 1961.

[35] T. D. Lee, K. Huang, and C. N. Yang. Eigenvalues and eigenfunctions of a Bose system of hard spheres and its low-temperature properties. *Phys. Rev. Lett.*, 106:1135, 1957.

[36] J. Steinhauer, R. Ozeri, N. Katz, and N. Davidson. Excitation spectrum of a Bose–Einstein condensate. *Phys. Phys. Lett.*, 88(12):120407, 2002.

[37] S. B. Papp, J. M. Pino, R. J. Wild, S. Ronen, C. E. Wieman, D. S. Jin, and E. A. Cornell. Bragg spectroscopy of a strongly interacting Rb85 Bose–Einstein condensate. *Phys. Rev. Lett.*, 101:135301, 2008.

[38] C. A. Sackett, J. M. Gerton, M. Welling, and R. G. Hulet. Measurement of collective collapse in a Bose–Einstein condensate with attractive interactions. *Phys. Rev. Lett.*, 82:876, 1999.

[39] S. Burger, K. Bongs, S. Dettmer, W. Ertmer, K. Sengstock, A. Sanpera, G. V. Shlyapnikov, and M. Lewenstein. Dark solitons in Bose–Einstein condensates. *Phys. Rev. Lett.*, 83(25):5198–5201, 1999.

[40] K. E. Strecker, G. B. Partridge, A. G. Truscott, and R. G. Hulet. Formation and propagation of matter-wave soliton trains. *Nature*, 417(6885):150–153, 2002.

[41] L. Khaykovich, F. Schreck, G. Ferrari, T. Bourdel, J. Cubizolles, L. D. Carr, Y. Castin, and C. Salomon. Formation of a matter-wave bright soliton. *Science*, 296(5571):1290, 2002.

[42] P. G. Drazin and R. S. Johnson. *Solitons: an introduction*. Cambridge University Press, 1989.

[43] G. Baym and C. J. Pethick. Ground-state properties of magnetically trapped Bose-condensed rubidium gas. *Phys. Rev. Lett.*, 76:6, 1996.

[44] K. W. Madison, F. Chevy, V. Bretin, and J. Dalibard. Stationary states of a rotating Bose–Einstein condensate: Routes to vortex nucleation. *Phys. Rev. Lett.*, 86:4443, 2001.

[45] F. Chevy, K. W. Madison, and J. Dalibard. Measurement of the angular momentum of a rotating Bose–Einstein condensate. *Phys. Rev. Lett.*, 85:2223, 2000.

[46] D. Guéry-Odelin and S. Stringari. Scissors mode and superfluidity of a trapped Bose–Einstein condensed gas. *Phys. Rev. Lett.*, 83(22):4452–4455, 1999.

[47] F. Zambelli and S. Stringari. Moment of inertia and quadrupole response function of a trapped superfluid. *Phys. Rev. A*, 63(3):33602, 2001.

[48] O. M. Maragó, S. A. Hopkins, J. Arlt, E. Hodby, G. Hechenblaikner, and C. J. Foot. Observation of the scissors mode and evidence for superfluidity of a trapped Bose–Einstein condensed gas. *Phys. Rev. Lett.*, 84:2056, 2000.

[49] O. M. Maragó, G. Hechenblaikner, E. Hodby, and C. J. Foot. Temperature dependence and frequency shifts of the scissors mode of a trapped Bose–Einstein condensate. *Phys. Rev. Lett.*, 86:3938, 2001.

[50] A. P. Chikkatur, A. Görlitz, D. M. Stamper-Kurn, S. Inouye, S. Gupta, and W. Ketterle. Suppression and enhancement of impurity scattering in a Bose–Einstein condensate. *Phys. Rev. Lett.*, 85:483, 2000.

[51] T. Frisch, Y. Pomeau, and S. Rica. Transition to dissipation in a model of superflow. *Phys. Rev. Lett.*, 69:1644, 1992.

[52] C. Raman, M. Köhl, R. Onofrio, D. S. Durfee, C. E. Kuklewicz, Z. Hadzibabic, and W. Ketterle. Evidence for a critical velocity in a Bose–Einstein condensed gas. *Phys. Rev. Lett.*, 83:2502, 1999.

[53] R. Onofrio, C. Raman, J. M. Vogels, J. R. Abo-Shaeer, A. P. Chikkatur, and W. Ketterle. Observation of superfluid flow in a Bose–Einstein condensed gas. *Phys. Rev. Lett.*, 85:2228–2231, 2000.

[54] S. Inouye, S. Gupta, T. Rosenband, A. P. Chikkatur, A. Görlitz, T. L. Gustavson, A. E. Leanhardt, D. E. Pritchard, and W. Ketter. Observation of vortex phase singularities in Bose–Einstein condensates. *Phys. Rev. Lett.*, 87:080402, 2001.

[55] T. Lahaye, C. Menotti, L. Santos, Lewenstein M., and T. Pfau. The physics of dipolar bosonic quantum gases. *Rep. Prog. Phys.*, 72(12):126401–126442, 2009.

[56] A. Griesmaier, J. Werner, S. Hensler, J. Stuhler, and T. Pfau. Bose–Einstein condensation of chromium. *Phys. Rev. Lett.*, 94:160401, 2005.

[57] Q. Beaufils, R. Chicireanu, T. Zanon, B. Laburthe-Tolra, E. Maréchal, L. Vernac, J. C. Keller, and O. Gorceix. All-optical production of chromium bose-einstein condensates. *Phys. Rev. A*, 77(6):061601, Jun 2008.

[58] R. E. Rosensweig. *Ferrohydrodynamics*. Cambridge University Press, 1985.

[59] T. Koch, T. Lahaye, J. Metz, B. Fröhlich, A. Griesmaier, and T. Pfau. Stabilizing a purely dipolar quantum gas against collapse. *Nature Physics*, 4:218–222, 2008.

[60] M. Lu, S. H. Youn, and B. L. Lev. Trapping ultracold dysprosium: a highly magnetic gas for dipolar physics. *Phys. Rev. Lett.*, 104(6):63001, 2010.

[61] R. Heidemann, U. Raitzsch, V. Bendkowsky, B. Butscher, R. Löw, and T. Pfau. Rydberg excitation of Bose–Einstein condensates. *Phys. Rev. Lett.*, 100:33601, 2008.

[62] J. Deiglmayr, A. Grochola, M. Repp, K. Mörtlbauer, C. Glück, J. Lange, O. Dulieu, R. Wester, and M. Weidemüller. Formation of ultracold polar molecules in the rovibrational ground state. *Phys. Rev. Lett.*, 101(13):133004, 2008.

[63] K. K. Ni, S. Ospelkaus, M. H. G. de Miranda, A. Pe'er, B. Neyenhuis, J. J. Zirbel, S. Kotochigova, P. S. Julienne, D. S. Jin, and J. Ye. A high phase-space-density gas of polar molecules. *Science*, 322(5899):231, 2008.

[64] J. G. Danzl, E. Haller, M. Gustavsson, M. J. Mark, R. Hart, N. Bouloufa, O. Dulieu, H. Ritsch, and H. C. Nagerl. Quantum gas of deeply bound ground state molecules. *Science*, 321(5892):1062, 2008.

[65] P. W. Anderson. Measurement in quantum theory and the problem of complex systems. In J. d. Boer, E. Dal, and O. Ulfbeck, editors, *The Lesson of Quantum Theory*, page 23, Amsterdam, 1986. Elsevier.

[66] A. J. Leggett and F. Sols. On the concept of spontaneously broken gauge symmetry in condensed matter physics. *Foundations of Physics*, 21:353, 1991.

[67] J. Javanainen and S. M. Yoo. Quantum phase of a Bose–Einstein condensate with an arbitrary number of atoms. *Phys. Rev. Lett.*, 76:161, 1996.

[68] Y. Castin and J. Dalibard. Relative phase of two Bose–Einstein condensates. *Phys. Rev. A*, 55:4330, 1997.

[69] J. I. Cirac, C. W. Gardiner, M. Naraschewski, and P. Zoller. Continuous observation of interference fringes from Bose condensates. *Phys. Rev. A*, 54:R3714, 1996.

[70] W. J. Mullin and F. Laloë. Interference of Bose–Einstein condensates: Quantum nonlocal effects. *Phy. Rev. A*, 78(6):061605, 2008.

[71] M. Albiez, R. Gati, J. Fölling, S. Hunsmann, M. Cristiani, and M.K. Oberthaler. Direct observation of tunneling and nonlinear self-trapping in a single bosonic Josephson junction. *Phys. Rev. Lett.*, 95(1):10402, 2005.

[72] S. Levy, E. Lahoud, I. Shomroni, and J. Steinhauer. The ac and dc Josephson effects in a Bose–Einstein condensate. *Nature*, 449(7162):579, 2007.

[73] J. Esteve, C. Gross, A.Weller, S.Giovanazzi, and M. K. Oberthaler. Squeezing and entanglement in a Bose–Einstein condensate. *Nature*, 455(7217):1216, 2008.

[74] M. F. Riedel, Pascal Böhi, Y. Li, T. W. Hänsch, A. Sinatra, and P. Treutlein. Atom-chip-based generation of entanglement for quantum metrology. *Nature*, 464:1170, 2010.

[75] C. Gross, T. Zibold, E. Nicklas, J. Estève, and M. K. Oberthaler. Nonlinear atom interferometer surpasses classical precision limit. *Nature*, 464:1165, 2010.

[76] O. Penrose and L. Onsager. Bose–Einstein condensation and liquid helium. *Phys. Rev.*, 104:576, 1956.

[77] E. W. Hagley, L. Deng, M. Kozuma, M. Trippenbach, Y. B. Band, M. Edwards, M. Doery, P. S. Julienne, K. Helmerson, S. L. Rolston, and W. D. Phillips. Measurement of the coherence of a Bose–Einstein condensate. *Phys. Rev. Lett.*, 83:3112, 1999.

[78] I. Bloch, T. W. Hänsch, and T. Esslinger. An atom laser with a cw output coupler. *Phys. Rev. Lett.*, 82:3008, 1999.

[79] K. Helmerson, D. Hutchinson, K. Burnett, and W. D. Phillips. Atom lasers. *Physics World*, page 31, August 1999.

[80] T. Donner, S. Ritter, T. Bourdel, A. Ottl, M. Köhl, and T. Esslinger. Critical behavior of a trapped interacting Bose gas. *Science*, 315(5818):1556–1558, 2007.

[81] M. Schellekens, R. Hoppeler, A. Perrin, J. Viana Gomes, D. Boiron, A. Aspect, and C. I. Westbrook. Hanbury Brown Twiss effect for ultracold quantum gases. *Science*, 310:648, 2005.

[82] T. Jeltes, J.M. McNamara, W. Hogervorst, W. Vassen, V. Krachmalnicoff, M. Schellekens, A. Perrin, H. Chang, D. Boiron, A. Aspect, and C. Westbrook. Hanbury Brown Twiss effect for bosons versus fermions. *Nature*, 445:402–405, 2007.

[83] M. Yasuda and F. Shimizu. Observation of two-atom correlation of an ultracold neon atomic beam. *Phys. Rev. Lett.*, 77:3090, 1996.

[84] E. Altman, E. Demler, and M. D. Lukin. Probing many-body states of ultracold atoms via noise correlations. *Phys. Rev. A*, 70:013603, 2004.

[85] S. Fölling, F. Gerbier, A. Widera, O. Mandel, T. Gericke, and I. Bloch. Spatial quantum noise interferometry in expanding ultracold atom clouds. *Nature*, 434:481–484, 2005.

[86] M. Greiner, C.A. Regal, J.T. Stewart, and D.S. Jin. Probing pair-correlated Fermionic atoms through correlations in atom shot noise. *Phys. Rev. Lett.*, 94:110401, 2005.

[87] Y. Kagan, B. V. Svistunov, and G. V. Shlyapnikov. Effect of Bose condensation on inelastic processes in gases. *JETP Lett.*, 642:209, 1985.

[88] E. A. Burt, R. W. Ghrist, C. J. Myatt, M. J. Holland, E. A. Cornell, and C. E. Wieman. Coherence, correlations, and collisions: What one learns about Bose–Einstein condensates from their decay. *Phys. Rev. Lett.*, 79:337, 1997.

[89] B. Laburthe Tolra, K. M. O'Hara, J. H. Huckans, W. D. Phillips, S. L. Rolston, and J. V. Porto. Observation of reduced three-body recombination in a correlated 1d degenerate Bose gas. *Phys. Rev. Lett.*, 92(19):190401, May 2004.

[90] R. E. Peierls. Quelques propriétés typiques des corps solides. *Ann. Inst. Henri Poincaré*, 5:177, 1935.

[91] N. D. Mermin and H. Wagner. Absence of ferromagnetism or antiferromagnetism in one- or two-dimensional isotropic Heisenberg models. *Phys. Rev. Lett.*, 17:1133, 1966.

[92] P. C. Hohenberg. Existence of long-range order in one and two dimensions. *Phys. Rev.*, 158:383, 1967.

[93] N. R. Cooper and Z. Hadzibabic. Measuring the superfluid fraction of an ultracold atomic gas. *Phys. Rev. Lett.*, 104(3):030401, 2010.

[94] I. Bloch, J. Dalibard, and W. Zwerger. Many-body physics with ultracold gases. *Rev. Mod. Phys*, 80(3):885, 2008.

[95] D. J. Bishop and J. D. Reppy. Study of the superfluid transition in two-dimensional ^{4}He films. *Phys. Rev. Lett.*, 40(26):1727–1730, 1978.

[96] V. L. Berezinskii. Destruction of long-range order in one-dimensional and two-dimensional system possessing a continous symmetry group - ii. quantum systems. *Soviet Physics JETP*, 34:610, 1971.

[97] J. M. Kosterlitz and D. J. Thouless. Ordering, metastability and phase transitions in two dimensional systems. *J. Phys. C: Solid State Physics*, 6:1181, 1973.

[98] D. R. Nelson and J. M. Kosterlitz. Universal jump in the superfluid density of two-dimensional superfluids. *Phys. Rev. Lett.*, 39:1201, 1977.

[99] N. V. Prokof'ev, O. Ruebenacker, and B. V. Svistunov. Critical point of a weakly interacting two-dimensional Bose gas. *Phys. Rev. Lett.*, 87:270402, 2001.

[100] V. S. Bagnato and D. Kleppner. Bose–Einstein condensation in low-dimensional traps. *Phys. Rev. A*, 44(11):7439–7441, 1991.

[101] Z. Hadzibabic and J. Dalibard. Two-dimensional Bose fluids: An atomic physics perspective. In R. Kaiser and D. Wiersma, editors, *Nano optics and atomics: transport of light and matter waves*, volume CLXXIII of *Proceedings of the International School of Physics Enrico Fermi, 2009*. IOS Press, 2010. arXiv:0912.1490.

[102] R. K. Bhaduri, S. M. Reimann, S. Viefers, A. Ghose Choudhury, and M. K. Srivastava. The effect of interactions on Bose–Einstein condensation in a quasi two-dimensional harmonic trap. *J. Phys. B: At. Mol. Opt. Phys.*, 33:3895, 2000.

[103] M. Holzmann, G. Baym, J. P. Blaizot, and F. Laloë. Superfluid transition of homogeneous and trapped two-dimensional Bose gases. *P.N.A.S.*, 104:1476, 2007.

[104] M. Holzmann and W. Krauth. Kosterlitz-Thouless transition of the quasi two-dimensional trapped Bose gas. *Phys. Rev. Lett.*, 100(19):190402, 2008.

[105] R. N. Bisset, M. J. Davis, T. P. Simula, and P. B. Blakie. Quasicondensation and coherence in the quasi-two-dimensional trapped bose gas. *Phys. Rev. A*, 79(3):033626, 2009.

[106] L. Giorgetti, I. Carusotto, and Y. Castin. Semiclassical field method for the equilibrium Bose gas and application to thermal vortices in two dimensions. *Phys. Rev. A*, 76(1):013613, 2007.

[107] S. T. Bramwell and P. C. W. Holdsworth. Magnetization: A characteristic of the Kosterlitz-Thouless-Berezinskii transition. *Phys. Rev. B*, 49(13):8811–8814, 1994.

[108] D. S. Petrov and G. V. Shlyapnikov. Interatomic collisions in a tightly confined Bose gas. *Phys. Rev. A*, 64:012706, 2001.

[109] A. Görlitz, J. M. Vogels, A. E. Leanhardt, C. Raman, T. L. Gustavson, J. R. Abo-Shaeer, A. P. Chikkatur, S. Gupta, S. Inouye, T. Rosenband, and W. Ketterle. Realization of Bose–Einstein condensates in lower dimensions. *Phys. Rev. Lett.*, 87:130402, 2001.

[110] P. Krüger, Z. Hadzibabic, and J. Dalibard. Critical point of an interacting two-dimensional atomic Bose gas. *Phys. Rev. Lett.*, 99(4):040402, 2007.

[111] Z. Hadzibabic, P. Krüger, M. Cheneau, S. P. Rath, and J. Dalibard. The trapped two-dimensional Bose gas: from Bose–Einstein condensation to Berezinskii–Kosterlitz–Thouless physics. *New Journal of Physics*, 10(4):045006, 2008.

[112] P. Cladé, C. Ryu, A. Ramanathan, K. Helmerson, and W. D. Phillips. Observation of a 2d Bose gas: From thermal to quasicondensate to superfluid. *Phys. Rev. Lett.*, 102(17):170401, 2009.

[113] A. Polkovnikov, E. Altman, and E. Demler. Interference between independent fluctuating condensates. *Proc. Natl. Acad. Sci. USA*, 103:6125, 2006.

[114] V. Gritsev, E. Altman, E. Demler, and A. Polkovnikov. Full quantum distribution of contrast in interference experiments between interacting one-dimensional Bose liquids. *Nature Physics*, 2:705–709, 2006.

[115] Z. Hadzibabic, P. Krüger, M. Cheneau, B. Battelier, and J. Dalibard. Berezinskii-Kosterlitz-Thouless crossover in a trapped atomic gas. *Nature*, 441:1118–1121, 2006.

[116] T. P. Simula and P. B. Blakie. Thermal activation of vortex-antivortex pairs in quasi-two-dimensional Bose–Einstein condensates. *Phys. Rev. Lett.*, 96:020404, 2006.

[117] S. Hofferberth, I. Lesanovsky, B. Fischer, T. Schumm, and J. Schmiedmayer. Non-equilibrium coherence dynamics in one-dimensional Bose gases. *Nature*, 449(7160):324–327, 2007.

[118] A. A. Burkov, M. D. Lukin, and Eugene Demler. Decoherence dynamics in low-dimensional cold atom interferometers. *Phys. Rev. Lett.*, 98(20):200404, 2007.

[119] E. A. L. Henn, J. A. Seman, G. Roati, K. M. F. Magalhães, and V. S. Bagnato. Emergence of turbulence in an oscillating Bose-Einstein condensate. *Phys. Rev. Lett.*, 103(4):045301, Jul 2009.

[120] W. S. Bakr, A. Peng, S. Folling, and M. Greiner. A quantum gas microscope for detecting single atoms in a Hubbard-regime optical lattice. *Nature*, 462:74–77, 2009.

[121] M. Greiner, M. O. Mandel, T. Esslinger, T. Hänsch, and I. Bloch. Quantum phase transition from a superfluid to a mott insulator in a gas of ultracold atoms. *Nature*, 415:39, 2002.

[122] N.R. Cooper. Rapidly rotating atomic gases. *Advances in Physics*, 57(6):539–616, 2008.

[123] L. E. Sadler, J. M. Higbie, S. R. Leslie, M. Vengalattore, and D. M. Stamper-Kurn. Spontaneous symmetry breaking in a quenched ferromagnetic spinor Bose–Einstein condensate. *Nature*, 443:312–315, 2006.

[124] M. Taglieber, A.-C. Voigt, T. Aoki, T. W. Hänsch, and K. Dieckmann. Quantum degenerate two-species Fermi-Fermi mixture coexisting with a Bose–Einstein condensate. *Phys. Rev. Lett.*, 100(1):010401, Jan 2008.

[125] J. Billy, V. Josse, Z. Zuo, A. Bernard, B. Hambrecht, P. Lugan, D. Clément, L. Sanchez-Palencia, P. Bouyer, and A. Aspect. Direct observation of Anderson localization of matter waves in a controlled disorder. *Nature*, 453:891, 2008.

[126] G. Roati, C. D'Errico, L. Fallani, M. Fattori, C. Fort, M. Zaccanti, G. Modugno, M. Modugno, and M. Inguscio. Anderson localization of a non-interacting Bose–Einstein condensate. *Nature*, 453:895, 2008.

[127] L. Sanchez-Palencia and M. Lewenstein. Disordered quantum gases under control. *Nature Physics*, 6(87), 2010.